

4-2019

An Evaluation of Sentinel-1 and Sentinel-2 for Land Cover Classification

Aaron Meneghini

Clark University, ameneghini@clarku.edu

Follow this and additional works at: https://commons.clarku.edu/idce_masters_papers

 Part of the [Geographic Information Sciences Commons](#), [Physical and Environmental Geography Commons](#), and the [Remote Sensing Commons](#)

Recommended Citation

Meneghini, Aaron, "An Evaluation of Sentinel-1 and Sentinel-2 for Land Cover Classification" (2019). *International Development, Community and Environment (IDCE)*. 235.

https://commons.clarku.edu/idce_masters_papers/235

This Research Paper is brought to you for free and open access by the Master's Papers at Clark Digital Commons. It has been accepted for inclusion in International Development, Community and Environment (IDCE) by an authorized administrator of Clark Digital Commons. For more information, please contact mkrikonis@clarku.edu, jodolan@clarku.edu.

An Evaluation of Sentinel-1 and Sentinel-2 for Land Cover Classification.

Author: Aaron Meneghini¹

¹Department of International Development, Community, and Environment. Clark University 950 Main Street, Worcester, MA. 01610. United States of America.

Date of Degree Conferment: May, 2019

A Master's Paper

Submitted to the faculty of Clark University, Worcester, Massachusetts, in partial fulfillment of the requirements for the degree of Master of Sciences in the department of International Development, Community, and the Environment.

**And accepted on the recommendation of
Dr. Florencia Sangermano, Chief Instructor**

Signature: _____

Abstract:
An Evaluation of Sentinel-1 and Sentinel-2 for Land Cover Classification.

Aaron Meneghini

This study evaluates Sentinel-1 and Sentinel-2 remotely sensed images for tropical land cover classification. The dual polarized Sentinel-1 VV and VH backscatter images and four 10-meter multispectral bands of Sentinel-2 were used to create six land cover classification images across two study areas along the border of the Bolivian Pando Department and the Brazilian state of Acre. Results indicate that Sentinel-2 multispectral bands possess a higher overall performance in delineating land cover types than the Sentinel-1 backscatter bands. Sentinel-1 backscatter bands delineated land cover types based on their surficial properties but did not facilitate the separation of similarly textured classes. The combination of Sentinel-1 and -2 resulted in higher accuracy for delineating land cover through increasing the accuracy in delineating the classes of secondary vegetation from exposed soil. While Sentinel-2 demonstrated the capability to consistently capture land cover in both case studies, there is potential for single date Sentinel-1 backscatter image to act as ancillary information in Sentinel-2 scenes affected by clouds or for increasing separability across classes of mixed multispectral qualities but distinct surficial roughness, such as bare ground versus sparsely vegetation areas.

Dr. Florencia Sangermano, Chief Instructor

ACADEMIC HISTORY

Name: Aaron Meneghini

Date: May 2019

Baccalaureate Degree: B.S. Environmental Science

Source: University of Massachusetts, Lowell

Date: May 2017

Occupation and Academic Connection since date of baccalaureate degree:

Clark University, M.S. in Geographic Information Science for Development and the Environment

Acknowledgements

I wish to thank my research advisor, Professor Florencia Sangermano, whose support, guidance, and encouragement enabled me to pursue this project. I am profoundly grateful for her expertise and patience and I consider it a privilege to have had the opportunity to work with her. I am also grateful to my family and friends, for their unwavering support throughout my academic career.

Table of Contents

List of Illustrations	
Tables	vi
Figures	vii
Introduction	1
Roles of Remote Sensing	2
Background of Synthetic Aperture Radar	2
Copernicus Program	4
Sentinel-2	5
Sentinel-1	7
Combing Sentinel-1 and -2	10
Research Goals	11
Methods	12
Results	17
Discussion	21
Conclusion	25
Figures	26
Literature Cited	44
Appendixes	47

List of Illustrations

Tables:

Table 1. Sensor Specifications for Sentinel-1 and Sentinel-2	26
Table 2. Data Products	26
Table 3. Case 1 Summary Table of Accuracy Assessment	43
Table 4. Case 2 Summary Table of Accuracy Assessment	44
Table 5. Confusion Matrices for Case Study 1	44
Table 6. Confusion Matrices Case Study 2	45
Table 8. Cross Tabulation Matrices, Case Study 1	46
Table 9. Cross Tabulation Matrices, Case Study 2	47

List of Illustrations

Figures:

Figure 1. Study Area Map	27
Figure 2. Case Study 1 and 2 False Color Composites	28
Figure 3. Training Site Locations	29
Figure 4. Training Site Backscatter Values – Case Study 1	30
Figure 5. Training Site Backscatter Values – Case Study 2	31
Figure 6. Spectral Signature Plots	32
Figure 7. Classification Results – Case Study 1	33
Figure 8. Classification Results – Case Study 2	34
Figure 9. Accuracy Assessment Points – Case Study 1	35
Figure 10. Accuracy Assessment Points – Case Study 2	36
Figure 11. Map Accuracy	37
Figure 12. Class Accuracy Case Study 1	37
Figure 13. Class Accuracy Case Study 2	38
Figure 14. Cross tabulation of Sentinel – 1 and Sentinel – 2 Classification Case Study 1	39
Figure 15. Cross tabulation of Sentinel – 1 and Sentinel – 1 and – 2 Classification Case Study 1	40
Figure 16. Cross tabulation of Sentinel – 2 and Sentinel – 1 and – 2 Classification Case Study 1	41
Figure 17. Cross tabulation of Sentinel – 1 and Sentinel – 2 Classification Case Study 2	42
Figure 18. Cross tabulation of Sentinel – 1 and Sentinel – 1 and – 2 Classification Case Study 2	43
Figure 19. Cross tabulation of Sentinel – 2 and Sentinel – 1 and – 2 Classification Case Study 2	44

1.1 Introduction

Accounting for nearly 30% of the world's land cover, forested ecosystems contain great quantities of the world's biodiversity, are fundamental providers of global ecosystem services, and are quintessential carbon sinks (Morley, 2000; Fagan and DeFries, 2009). Over the past 25 years, these ecosystems have been experiencing net losses as forests are degraded and transformed for anthropogenic use, particularly in tropical regions (FRA, 2015; UNFCCC, 2014; Müller et al., 2014). This landscape transformation has large impacts on biodiversity through changing habitat availability and straining established biogeochemical cycling (Skinner and Murk, 2011). At regional scales deforestation represents a significant loss in carbon reservoirs, without which, the effects of greenhouse gases would be substantial on global climate, through carbon introduction into atmospheric cycling (Skinner and Murk, 2011; Rahman M. and Tetuko Sri Sumantyo J., 2010).

Given the essential roles played by forest ecosystems on regional and global scales, international concerns have been raised over the effects of net forest loss due to clear-cut deforestation and forest structure degradation (UNFCCC, 2014). To mitigate the potentially disastrous effects of climate change and biodiversity loss, the program "*Reducing Emissions from Deforestation and Forest Degradation*" (REDD+) was instituted by the United Nations Framework Convention on Climate Change (UNFCCC) (Pistorius et al 2012; UNFCCC, 2014). Countries participating in this voluntary program have the potential to receive economic benefits for reducing deforestation and degradation in their country (UNFCCC, 2014). However, the dispersal of these financial incentives are reliant on the quantification of national carbon inventories through measurement, reporting and verification systems (MRVs) (Mitchell et al. 2017). These systems are built through the operational implementation of satellite earth observation missions complemented by ground-based forest assessments (Mitchell et al., 2017; Violini, 2013).

1.2 Roles of Remote Sensing:

For almost 40 years, optical satellite missions such as Landsat, Landsat Thematic Mapper, Satellite Pour l'Observation de la Terre (SPOT), and the Moderate Resolution Imaging Spectroradiometer (MODIS), have been used to capture and quantify land cover globally (Mitchell et al. 2017). These missions operate through optically capturing the visible to shortwave infrared wavelengths of the electromagnetic spectrum (Mitchell et al. 2017; Joshi et al., 2016). As they pass over landscapes, these optical platforms scan illuminated objects through push broom, line scanner, or framing camera sensors (Warner, 2009; Chuvieco, 2016). For REDD+ mapping and other monitoring projects, the scanned images are transformed into maps of discrete and quantified land cover classes through classification techniques.

Despite the global implementation of optical platforms, challenges remain for capturing scenes of regions effected by persistent cloud cover (Haack and Mahabir 2018). To capture areas affected by persistent cloud cover, sensors can comprise between high revisit time and spatial resolution, where a higher sensor revisit time enables the acquisition of cloudless scenes at the cost of spatial resolution (Warner, 2009). However, there is potential for meeting these requirements with recent developments of synthetic aperture radar (SAR) and high spatial resolution multispectral satellite constellations (Mitchell et al. 2017).

1.3 Background of Synthetic Aperture Radar (SAR):

SAR platforms can penetrate cloud cover and observe negligible atmospheric effects, especially in wavelengths that are greater than 3 centimeters (Chuvieco, 2016; Smith, 2012). This capability shows promise for monitoring regions that are persistently covered by clouds. Side-looking SAR sensors capture images of landscapes through emitting and receiving an electromagnetic pulse between 0.1 centimeters and 1 meter (Fernandez-Ordonez, 2009). The emitted pulse scatters upon interacting with objects, resulting in a signal of returned energy, which is captured by the sensor (Chuvieco, 2016; Smith, 2012).

SAR processing techniques use the returned signal to inform upon both the duration of time between emission and reception as well as the intensity of the backscatter return (Chuvieco, 2016). The time between the emitted pulse and receiving signal relates to distance from the sensor to the terrain (Smith, 2012). The intensity of the returned signal relates to the microwave pulse land cover interactions (Chuvieco, 2016). This is formulated through the equation below:

$$P_r = \frac{P_1 G^2 \lambda^2 \sigma}{(4\pi)^3 r^4}$$

(P_r) reflected backscatter power

(P_1) radar emission power

(G) the antenna gain factor

(r) the distance between the terrain and the platform

(λ) the electromagnetic wavelength of the emitted pulse

(σ) the backscatter coefficient through the equation

Equation (1) (Chuvieco 2016)

Before informing upon land cover, the intensity values must be converted into their respective backscatter values (Chuvieco, 2016). These backscatter values vary between different land cover types and may be used in image analysis for land cover monitoring (Smith, 2012).

The major governing factors controlling the backscatter intensities of radar are the surficial roughness qualities of the land cover, slope facing in relation to the satellite view angle, moisture content, and the elevation of terrain especially in scenes with dramatic relief (Fernandez-Ordonez, 2009; Smith, 2012). Higher backscatter is typically observed in areas of rough surficial qualities or in slopes facing towards the view angle of the satellite while lower backscatter is typically observed in areas of smooth surficial qualities or slopes facing away from the view angle of the satellite (Chuvieco, 2016; Smith, 2012). Thus, when the slope and topographic qualities are known, radiometric calibrations can be performed to isolate the surficial roughness of land cover.

Inferences pertaining to land cover have been seen to vary in performance across microwave bands (Kasischke et al., 1997). For instance, C-band wavelengths are short enough that they interact and

scatter at the canopy level of vegetation whereas longer wavelengths experience this type of scattering (termed volume scattering) in forest sub canopy structure (Smith, 2012; Mahmudur Rahman and Tetuko Sri Sumantyo, 2009). Differences in scattering over land cover types, and thus backscatter intensity, can be analyzed landscape analysis (Fernandez-Ordonez et al., 2009).

While they operate in only a single electromagnetic microwave band, unlike the multispectral band resolution of optical sensors (Warner, 2009; Chuvieco, 2016), SAR sensors are able to acquire images at different polarizations. Polarization refers to the “locus of the electric field vector in the plane perpendicular to the direction of propagation of the microwave radiation” (Fernandez-Ordonez et al. 2009). Both the emitted and scattered receiving pulses from SAR satellites are either polarized vertically or horizontally (V or H) resulting in potential polarization combinations of HH, VV, HV, and VH (Fernandez-Ordonez et al., 2009). Sensors can either acquire single polarization combinations or multiple polarization combinations where a single polarization could acquire HH or VV; a dual polarization sensor can acquire HH and HV, VV and VH, or HH and VV; and quad polarization sensor can acquire HH, VV, HV, and VH (Fernandez-Ordonez et al., 2009; Smith, 2012).

Previous constraints to SAR applications in deforestation and land cover mapping were due to the single polarization of previous SAR datasets (T. Idol et al. 2015). More recently, multi-polarized sensors such as Copernicus program Sentinel-1 satellites have been launched as active earth observation constellations. The promise of these multi-polarized radar sensors is the greater acquisition of surficial properties in relation to different polarizations, and thus they represent a greater potential to capture land cover physical characteristics (Shearon & Haack, 2013; Sawaya et al, 2010; Mahmudur Rahman and Tetuko Sri Sumantyo, 2009).

1.4 Copernicus Program:

Recently, two new satellite missions have been launched as part of the European Union’s earth observation initiative Copernicus. The Sentinel-1 and Sentinel-2 missions have the objective to monitor

earth biophysical and land cover qualities using both radar and high resolution optical platforms (ESA 2014). Both missions are satellite constellations where Sentinel-1 is comprised of, Sentinel 1A and Sentinel 1B and Sentinel-2 is comprised of Sentinel-2A and Sentinel-2B. Sentinel-1 was the first mission of the two, where Sentinel-1A was launch in April 2014 and followed by Sentinel-1B in April 2016. Only a year after the launching of the Sentinel-1 mission, the first satellite of the Sentinel-2 mission, Sentinel-2A, was launched in June 2015 and followed by Sentinel-2B in March 2017.

1.5 Sentinel-2

The sun-synchronous polar-orbiting Sentinel-2 satellites have a temporal resolution of 10 days with one satellite and 5 days with two satellites, between the latitudes of 84° North and 56° South (ESA, 2015). Equipped with a push-broom sensor called the MultiSpectral Instrument (MSI), Sentinel-2A and Sentinel-2B capture 13 total spectral bands. At 10 meter spatial resolution 4 bands capture the visible and near infrared sections of the electromagnetic spectrum, at 20 meter spatial resolution 6 bands capture the near to shortwave infrared wavelengths of the electromagnetic spectrum, and 3 bands at a 60 meter spatial resolution at the blue, near infrared, and shortwave infrared sections of the electromagnetic spectrum (ESA, 2015).

This satellite distributes data products in two levels, 1C and 2A, where 1C captures the Top-Of-Atmosphere reflectance and 2A captures Bottom-Of-Atmosphere reflectance, through the open access data hub Copernicus. With the overall lifespan of a Sentinel-2 satellite being projected to be around 7 years and the planned additions to the constellation, this satellite mission is a prominent new addition to the field of remote sensing (Mitchel et al., 2017).

Recognizing the potential this satellite represents for the future of land cover monitoring, studies have worked to evaluate Sentinel-2 for land cover classification through case studies (Li and Roy, 2017). Varying from land cover classification to biomass estimation, Sentinel-2 has demonstrated

promising potential for earth observation (Marangoz et al., 2017; Wang et al, 2018; Thanh Noi and Kappas 2018; Forkuor et al., 2017; and Carrasco et al., 2019).

For example, enabled by the similarities between the Sentinel-2 and Landsat-8 missions Mandanici and Bitelli (2016), Magangoz and Skertekin (2017) compared the differences between Landsat-8 land cover classification and Sentinel-2 land cover classification through object-based classification methods and evaluated the respective accuracies through the Kappa statistic. They reported higher accuracies in land cover classification for Sentinel-2 than Landsat-8 in their study area of Zonguldak near the Western Black Sea of Turkey. They conclude that possible reasons for the improved accuracy could be due to the higher spatial resolution of Sentinel-2 which outperformed the pan sharpened 15 meter resolution bands of Landsat-8. This high performance of Sentinel-2 for land cover classification accuracy was complemented by the work of Carrasco et al. (2019), who showed temporally aggregated Sentinel-2 composite images had slightly higher land cover classification accuracy compared to Landsat-8 temporal composites.

Using Sentinel-2 MSI spectral bands in a random forest (RF) model, in the Hebei province of China, Wang et al. (2018) determined that the MSI spectral sensor could accurately estimate fractional vegetation cover and that, through iterative variable modeling, the most important Sentinel-2 bands influencing model accuracy were 4 (red), 8a (near infrared), and 12 (shortwave infrared); highlighting what many studies have otherwise omitted, band importance for estimation of vegetation cover.

Following this work, Thanh Noi and Kappas (2018) evaluated the use of RF as a classifier for Sentinel-2 and compared to other classification methods. They found that all non-parametric classifiers produced high accuracies (near 90 to 95%), with Support Vector Machines (SVM) producing the highest accuracies followed by RF and KNN respectively. Their results differ from the results seen by Clerici et al. (2017) whom reported lower Sentinel-2 map classification accuracies, some of which were near 50%. It should be noted though, that Clerici et al. (2017), omit the number of trees used, which Thanh Noi and

Kappas (2018) found to have large impacts on accuracy and that Clerici et al (2017) implemented an object based method.

The studies mentioned above begin to describe the overall potential of the Sentinel-2 mission through demonstrating high classification accuracy in a range of geographic areas. However, despite the potential of the Sentinel-2 constellation for land cover and land use monitoring; optical sensors in general, are constrained by cloud cover and sun illumination (Joshi et al., 2016; Chuvieco, 2016; Warner et al. 2009). Given these constraints, optical based land cover classification can face challenges in regions that experience frequent cloud cover (Chuvieco, 2016), such as tropical environments (Skinner and Murck, 2011).

1.6 Sentinel-1

Sentinel-1 provides new opportunities to employ the advantages of SAR backscatter to image analysis techniques through the dual polarization C-band platform (Haack and Mahabir 2018; Torres et al., 2012). With a 12 day repeat cycle, the Sentinel-1 platform is a C-band (5.4 GHz) SAR satellite with dual polarization modes of acquisition in the VH and VV amplitude bands acquiring amplitude and phase information in slant range geometry (Torres et al., 2012). Using these polarization bands, there are multiple forms of acquisition modes that Sentinel-1 provides data in; a level 1 product known as the single look complex (SLC) and a level 2 product known as a ground range detected (GRD) product (Torres et al., 2012). The Sentinel-1 SLC images are constructed by sub swaths constituting the 250 km image extent at initially 5 meters by 20 meters, a spatial geometry termed slant range geometry, which is a line of sight from the side looking radar platform to the reflectance object (Torres et al., 2012). In SAR applications, a single look image implies that there has been no pixel averaging whereas an image that has experienced two looks would possess pixels created through an average of 2 by 2 pixels (Funing 2018).

The SLC data format provides information concerning the amplitude of the backscatter intensity and the phase in the backscatter as well; which can translate into time of return (Funning, 2018). Dense temporal image stacks of these SLC images can and have been used to monitor change in a landscape through calculating phase differentials (Funning, 2018). These methods can be used for studying land change through analyzing land subsidence and deformation, linked to geomorphological processes (Funning, 2018). SLC images can also be used in coherence matrix estimates to compare and quantify the relationship between phase and amplitude values captured in multiple SLC images (Smith, 2012). The Sentinel-1 GRD products are created through merging and combining the SLC products, and projected to a ground range using the Earth Ellipsoid model WGS 1984. The main difference between these two data products is the loss of the phase information in the GRD product. In terms of the analytical capabilities for GRD image, the loss of phase information prevents analysis pertaining to InSAR change analysis (Funning, 2018) but enables the use of more wide spread land cover and land change analytical techniques through analyzing the different scattering relationships from land cover class to land cover class (Smith, 2012)

Only a few recent studies have implemented the Sentinel-1 SAR platform in land cover analysis and even fewer with the focus on analyzing tropical deforestation and land cover (Schumillis 2015). Additionally, of the studies conducted with Sentinel-1, most examined SAR time series for land cover monitoring over a season or annual period. For example, Johannes Reiche et al. (2018) conducted a comparative study between Sentinel-1, Landsat, and ALOS-2 PALSAR-2 which demonstrated the exceptional ability for Sentinel-1 to detect deforestation in low land dry forest Bolivia (South east of Santa Cruz) earlier than Landsat and ALOS-2 PALSAR-2 in the context of near real time (NRT) deforestation monitoring. The specific datasets and methodology used by Reiche et al. (2018) included a Sentinel-1 VV-polarized C-band dataset, a PALSAR-2 HV-polarized L-band dataset, and Landsat 7 and 8 (ETM+ and OLI) NDVI time series datasets between 10/01/2017 through 9/30/2016, where the first year

was used as training and the second year was used to detect deforestation. Overall, they found that Sentinel-1 was an integral part of their NRT system, multi-sensor detection greatly increased deforestation detection, and that there is great opportunity in utilizing Sentinel-1 for deforestation detection (Reiche et al. 2018).

For land cover classification, Dostalova et al. (2016) studied the accuracy of a single season Sentinel-1 time series for creating a forest mask in Burgenland, Austria using K-means clustering analysis. They reported producer, user, accuracy statistics above 85% with Kappa statistics upwards of 0.77. Another study, conducted by Balzter et al., 2015, evaluated combined Sentinel-1 HH, HV, VV, VH, and HH polarization bands across multiple dates with ancillary data sources such as a digital terrain model, for CORINE (a standardized European class convention) land cover mapping in Thuringia, Germany. They found a classification accuracy 68.4% for mapping CORINE land cover through a random forest classification method (Balzter et al., 2015). This multi-temporal SAR image analysis was built off of work which reported high classification accuracies (greater than 90%) through decision tree classification of multi-temporal C-band SAR images derived from ENVISAT ASAR AP and ERS-2 in the same region of Germany but with the classes of water, grassland, agriculture, forest, and settlement (Thiel et al., 2009).

Very few studies have explored the use of single Sentinel-1 dual polarized image for land cover classification potential. Abdikan et al. (2016) demonstrated the application of single date Sentinel-1 dual polarization bands in land cover classification of the greater Istanbul province in Turkey, through support vector machine classification. They separated water, urban settlements, pure and mixed forests, agriculture, and bare land, through iterated classifications of the Sentinel-1 backscatter images VV, VH, VV VH image difference, and VV VH image quotient. The investigators reported varying accuracies with the highest observed overall accuracies reaching near 93% and input bands of VV, VH, and VV VH quotient. The high accuracies reported by Abdikan et al. (2016) are contrasted against the

map accuracies reported by Clerici et al. (2018), in their Colombian case study. As part of their study, Clerici et al. (2018) observed poor classification map accuracies of single date Sentinel-1 VV and VH texture bands in random forest, support vector machine, and K-Nearest Neighbor classifiers. Considering the variable classification accuracies reported by investigators and the potential benefit of utilizing SAR imagery in persistently cloud covered regions, further evaluation is needed to characterize the performance of single date Sentinel-1 images for land cover classification applications.

1.7 Sentinel-1 and Sentinel-2 Integration:

Studies have worked on combining SAR and optical data sources to incorporate remote sensing information that relies on different physical and biochemical principles, recognizing that this data model produces a more holistic data description of land cover types and has great potential for increasing land cover classification accuracy (Joshi et al., 2016). Haack and Mahabir (2018) explored the optimal band for land cover mapping (for classes ranging from agricultural to other anthropogenic land cover classes), of both optical and SAR data; utilizing Landsat and PALSAR-L band dual-polarization imagery. Referencing this radar data, they derived multiple texture measures for each polarization band (Haack and Mahabir 2018). The investigators found that based off divergence analysis (Swain et al. 1981), the Landsat TM red band demonstrated the most separability within their Peru case study; the red band was followed closely in separability value by the RADARSAT HH variance texture. Haack and Mahabir (2018) elaborate that a potential reason for this result of optimally selected bands is due to the land cover classes in the study area.

In Colombia, integration of Sentinel-1A with Sentinel-2A, was done as an exploratory analysis comparing the land cover classes of forests, secondary vegetation/shrubs, cropland, water, pastureland, and built areas, through SVM, Random Forest, and K-Nearest Neighbors (Clerici et al., 2017). The investigators preprocessed and resampled the bands from Sentinel-1 and Sentinel-2 to 10 meters by 10 meters in the Sentinel Application Platform (SNAP); where the SAR images were used to calculate grey

level co-occurrence texture qualities (Haralick, Shanmugat, and Dinstein, 1973). The resulting band combination of SAR backscatter bands, SAR texture bands, and optical bands were segmented through eCognition before being run through the three non-parametric classifiers.

SVM demonstrated the highest overall accuracy for the integrated Sentinel radar and optical images with an overall accuracy of 88.75% followed by Random Forest at 55.5% and k-Nearest Neighbor at 39.37% (Clerici et al., 2017). Individually, Sentinel-1A observed a 30.62%, 20.12%, and 16.98% overall accuracy in each of the classifiers respectively; whereas Sentinel-2A observed accuracies ranging from 72.5%, 48.1%, and 37.15% in SVM, Random Forest, and k-Nearest Neighbor, respectively (Clerici et al., 2017). The study reported that the greatest omission and commission to be found in crops and secondary vegetation, however did not report upon other class accuracies. The authors note that a limitation of their approach is the object definition through eCognition limits and complicates automated map development and operational implementation of this method (Clerici et al., 2017). However, the authors note, that the primary advantage of using Sentinel-1 and Sentinel-2 in conjunction is the SAR benefit of image acquisition regardless of weather conditions and the SNAP preprocessing platform facilitates automated processing of both data products; however they specify that more research is needed to examine the potential and benefit in combining these two sensors.

1.8 Research Goals:

There has been demonstrated success in land cover mapping for Sentinel-2 across different case studies in the world. Sentinel-1 has shown promise in land cover mapping and land cover quantitative analysis. Combined the two have been shown to produce higher classification accuracies than either achieved alone. Given the promise of using Sentinel-1 to quantitatively track and evaluate land cover and the high classification accuracy of Sentinel-2, the aim of this work is to evaluate, individually and combined, the satellites Sentinel-1 and Sentinel-2 for operational tropical land cover mapping.

2. Methods:

2.1 Study Area:

This work was split between two case studies which were centrally located in the Bolivian Pando Department, where case study 1 overlaps with the neighboring state of Acre, Brazil (figure 1 and 2). Case study 1 captures a residential area in the Placido de Castro municipality of Acre, Brazil, to the northwest of the scene. The Abuna river divides the two neighboring countries and the dominant land cover types are primary forest, bare land and secondary vegetation. Case study 2 is completely contained within the Bolivian Pando department, several miles south of case study 1, depicting a dominantly forested landscape with patches of deforestation in varying levels of regrowth.

The data products listed in table 2 were downloaded from the ESA data hub website Copernicus, where Sentinel-1 and -2 imagery can be publicly accessed and downloaded.

2.2 Sentinel-2A-MSI Preprocessing:

The .SAFE Sentinel-2 MSI data product was atmospherically corrected through the Rayleigh correction operator version 1.3 in the Sentinel-2 toolbox. This operator's general processing chain estimates Rayleigh reflectance, calculates Rayleigh transmittance, and then each pixel's apparent reflectance is corrected for its Rayleigh contribution (Bourg 2009). The parameters of the operator were specified as follows: Sea level pressure in hPa and Ozone in DU were left at the MSI default values of 1013.25 hPa and 300 DU respectively. The output product of bottom of Rayleigh reflectance was selected for the four 10-meter bands of Sentinel-2 (see table 1) and exported as a GeoTiff.

2.3 Sentinel-1 Preprocessing:

The Sentinel-1 GRD product was used in this work and the following SAR imagery pre-processing steps conducted in the Sentinel Application Platform (SNAP) were: orbit correction, radiometric calibration, speckle reduction, geometric terrain correction, and band mathematical operations.

2.3.1 SAR Backscatter Calibration:

Radiometrically calibrating the amplitude bands into sigma nought backscatter values for Sentinel-1 is calculated for each pixel through equation 2:

$$i = \frac{|DN_i|^2}{A_i^2}$$

Equation (2)

where value of (i) is determined by look up tables accompanying the level 1 products, A_i is equal to either $\beta_{Nout}(i)$ or $\sigma_{Nought}(i)$, and points that fall between pixels are bilinearly interpolated (Laur et al. 2004). This calibration was run on both VV and VH amplitude bands and sigma nought backscatter output bands were created.

2.3.2 SAR Speckle Filter:

After calibration, a speckle filter was applied to reduce the inherent noise present in SAR data caused by the random constructive and destructive interference of radar waves (Mansourpour et al 2006; Smith, 2012; Mahmudur Rahman and Tetuko Sri Sumantyo, 2009). Many speckle filters exist and are implemented with two objectives, (1) to reduce the pixel value variability within a radar derived image while (2) simultaneously attempting to preserve radiometric qualities of features (Mansourpour et al. 2006; Smith, 2012). The adaptive filter Lee-sigma was used as due to its capacity for suppressing speckle while preserving textural information (Qiu et al. 2004, Lee et al. 1994). The Lee-sigma filter calculates, through a specified moving kernel, the output DN value of a pixel as the average of all values that fall within 2 standard deviations of range of local pixels (Lee 1983). The effect of this filter, is that DN values will be altered to those surrounding them that fall within two standard deviations of the range of pixels. The Lee-sigma filter was run on the sigma naught calibrated VV and VH backscatter bands used a kernel window size of 5 pixels by 5 pixels, a default sigma value of 0.9, a target window size of 3 pixels by 3 pixels and was specified to be single look.

2.3.3 SAR Terrain Correction:

The output filtered bands were then geometrically corrected through Range Doppler orthorectification following the method by Small and Schubert (2008). This method pulls from both the radar metadata and a reference digital elevation model (DEM) to correct for distortions in distance created due to both topographical variations in a landscape and the look angle of the sensor. The Shuttle Radar Topography Mission (SRTM) elevation model at 3 arc second resolution was used as the reference DEM while the output pixel spacing of 10 meters was preserved through Bilinear Interpolation. The output product contained geometrically corrected SAR VV and VH bands at 10 meters by 10 meters with a coordinate system of WGS 1984.

2.3.4 Band Manipulation and Data Export:

Both VV and VH bands were converted to a logarithmic scale. Because of the success reported by Abdikan et al (2016) when they included a manipulated quotient band for land cover classification, an additional band was created through the division of the VV and VH polarization bands. All bands were projected from WGS 1984 to Universal Transverse Mercator (UTM) zone 19 South, matching the projected coordinate system of the Sentinel-2 MSI product.

2.5 Image classification:

Having demonstrated a high performance with Sentinel-2 land cover classifications (Thanh Noi and Kappas, 2018) a random forest (RF) decision tree classification method was used for this work. Random forest is a non-parametric classification method requiring no standardization across inputs (Hansen et al. 1996), facilitating classification of data products ranging from SAR imagery, optical imagery, integrated SAR and optical imagery, and or other ancillary data products such as DEMs.

Fundamentally, a random forest is composed of a collection of decision trees (Breiman 2001). Where a single decision tree is a structure created through recursive partitioning, splitting datasets into homogenous groups (Breiman 2001). Key splits are created through sequential sets of binary rules that characterize datasets (Chuvieco, 2016). In a classification context, these rules can be thresholds of

spectral reflectance or backscatter intensity or based on categorical ancillary information (Chuvieco, 2016). While flexible in terms of inputs, decision trees can face challenges of overfitting, which reduce model accuracy (Breiman 2001). Through combining these decision trees in a Random Forest, key splits and key variables can be voted on for best contribution to the model, thus mitigating model error from overfitting (Breiman, 2001).

Of the outputs produced from random forest this study utilized the confidence image for iterative classification training. The confidence image assigns each pixel with the model probability, ranging from 0 to 1, of a pixel being classified correctly. Using this confidence, poorly modeled and predicted classes across the scene can be visually identified through patches of low confidence. Areas of low confidence were then supplied additional training sites in an iterative classification process to better capture the class variability throughout the scene.

For each case study, training sites were used input into the Classification and Regression Training (caret) R package, to train the Random Forest ensemble classification method (Kuhn, 2008). From the training sites, all training site pixels were extracted to compose the model sample size and 1000 trees constituted the random forests. After the iterative classification procedure, three final random forest models were selected for the Sentinel-1 image classification, Sentinel-2 image classification, and the combined Sentinel-1 and Sentinel-2 image classification.

The Sentinel-1 RF model used the bands the VV, VH, and quotient band of VV and VH as inputs. The inclusion of these bands was informed by the high performance observed with these bands for land cover classification by Abdikan et al (2016). The Sentinel-2 RF model used the blue, green, red, and near infrared bands to their high spatial resolution and the high classification importance of Sentinel-2's red and near infrared bands observed by Wang et al. (2018). Lastly, the integrated Sentinel-1 and Sentinel-1 RF model used both the SAR backscatter bands and multispectral optical bands as inputs.

2.6 Training Sites:

In Quantum GIS (QGIS), both true and false color composites created from Sentinel 2 were used and compared against high resolution google earth historical imagery to identify training sites for both case studies. Motivated by the goal to separate the most prominent land cover features into broad categories, for the first case study scene classes were delineated to separate structures and paved roads (termed residential), secondary vegetation, dense forest cover, bare ground, and water.

Training sites were iteratively developed through interpreting multiple random forest classification confidence images highlighting areas exhibiting uncertainty. For case study 2, the residential class was removed due to the absence of discernable urban objects in the MSI imagery, however, due to the presence of two small secluded rivers, water was preserved as a class. Figure 3 shows training site locations for each case study respectively, these training sites were digitized at the 10-meter level, in some cases identifying individual pixels for pure class examples.

2.7 Accuracy Assessment and Map Comparison:

Two steps composed post image classification evaluation, map error and map cross tabulation. Map error was calculated for each final random forest model through sampling each class. With these points, the ground truth class was recorded through the evaluation of historical google earth imagery corresponding to July 2018 and Sentinel-2 False Color Composites. The point attributes, tabulating classification and ground-truth classes, were used to evaluate the overall classification and class accuracy through the calculation of a confusion matrix. From the confusion matrix, image overall accuracy, class accuracy, and errors of omission and commission, were calculated. The overall accuracy referred to the percentage of sampled pixels correctly classified, while the class accuracy referred to the percentage of sampled pixels correctly classified in a specific class. An error of omission indicated that a class had not fully included features of that class, while an error of commission indicated a class incorrectly included features belonging to a different class. These metrics were used to evaluate the error of the Sentinel-1, Sentinel-2, and combined Sentinel-1 and -2 classification images.

The second evaluation of the classification images was conducted through map cross tabulations. The map cross tabulations highlighted the agreement and disagreement across class allocation across the three final random forest classifications. The agreement and disagreement were then used to comment on class similarity and key class dissimilarity.

4. Results:

Analysis of Separability:

Across inputs, the training sites extracted the statistical character of classes. This character, also referred to as class signatures, is the basis for effective land cover classification (Chuvieco et al. 2016). When there are large overlaps in the mean and standard deviation of class signatures, classification error can occur due to low class separability (Chuvieco et al. 2016). Thus evaluating class signatures, either graphically or mathematically, can quantify the degree to which a class is discernable from another class (Chuvieco et al. 2016). Across both case studies, the final class signatures derived from Sentinel-1 VV and VH backscatter polarization inputs demonstrated larger inter-class overlaps than the final class signatures for Sentinel-2 multispectral reflectance (figures 4, 5, and 6).

The overlap of Sentinel-1 backscatter signatures, was observed in two groups of classes, rough surfaced classes and smooth surfaced classes. With relatively high backscatter values, the rough surfaced classes of forest, secondary vegetation, and residential experienced significant overlap across the VV and VH polarizations (figure 4 and 5). With relatively lower backscatter values, the smooth surfaced classes of water and exposed soil also experienced significant overlap in the VV and VH polarizations (figure 4 and 5). However, while within these two groups separability was low, between these two groups, separability was high (as rough surfaced classes exhibited higher VV and VH backscatter than smooth surfaced classes). This indicated that surficial roughness of classes was the dominate actor in separability when using single date Sentinel-1 VV and VH polarization images.

Across the Sentinel-2 bands, overlap between signatures was significantly lower than seen across the Sentinel-1 VV and VH bands (figure 6). The greatest overlap between spectral signatures was seen between the classes of forest, exposed soil, and secondary vegetation across the blue, green, red, and near infrared bands. This indicated that the classes that were biophysically most similar, capturing varying degrees of vegetation, were the least separable. The water class signature demonstrated high reflectance values in case study 2. The high near infrared reflectance values observed in the water class of case study 2 highlighted the presence of obscuring vegetation, resulting in a mixed class signature.

The class signatures of both Sentinel-1 VV and VH backscatter and Sentinel-2 spectral reflectance were used to classify the combined Sentinel-1 and Sentinel-2 classification.

4.1 Classification Images

4.1.1 Sentinel-1 Classification

Across case studies, both the low overall accuracy and class accuracies were coupled with high omission and commission errors observed in the Sentinel-1 classification images. These high errors highlighted the poor signature separability between classes of similar roughness. Despite the low measured accuracy of the Sentinel-1 classification images, general geographic patterns of the scenes were captured through the classes of exposed soil and forest. The classes of exposed soil and forest delineated the landscapes by rough and smooth features (figure 7). The classes of residential, secondary vegetation, and water were speckled throughout the images, with little contiguity. This speckling of the classes residential, secondary vegetation, and water resulted in error that lowered overall accuracy of case study 1 and 2, to 55% and 38% respectively (table 5 and 6).

The accuracies were highest for the classes of forest (at 90% and 94%) and exposed soil (at 68% and 50%) but dropped considerably in the classes of secondary vegetation, residential, and water. The classes of secondary vegetation, residential, and water all showed accuracies between 5% and 50% across each case study. These low accuracies in the rough surfaced classes of residential and secondary

vegetation were related to high commission errors predominately linked to omission in the class of forest. Spatially, this manifested itself through speckled distributions of the two classes inside core forest areas. Similarly, the smooth surfaced classes of case study 1 (water and exposed soil), resulted in shared commission and omission errors between the classes. This supported the class backscatter signature evaluation, where classes of similar surficial roughness demonstrated significant overlap and low separability.

One prominent exception to error being based on surficial class roughness was the speckled distribution of the exposed soil class throughout homogenous forested areas. These classes of opposing surficial roughness experienced errors of commission and omission (table 5). Visually, this was captured in the forest backscatter signature (figure 4 and 5) and in the Sentinel-1 VV and VH backscatter polarization false color composite, where regions of homogenous land cover were often described by heterogeneous pixel values of neighboring high and low backscatter values despite belonging to one class. This heterogeneity of high and low backscatter intensity resulted in the speckled distribution of exposed soil in core forest.

Overall, the overlaps in Sentinel-1 VV and VH polarization backscatter signatures resulted in lower classification capabilities for delineating the classes of similar surficial qualities. Speckle commonly found in SAR imagery introduced further confusion due to the heterogeneity of pixel backscatter intensities in homogenous land covers.

4.1.2 Sentinel-2 Classification Image

The higher class separability observed across the blue, green, red, and near infrared bands of Sentinel-2 resulted in classification images with lower errors of omission and commission across classes and higher overall accuracies of 74% and 68%, for case studies 1 and 2 respectively (figure 11). The classes of forest, exposed soil, and water showed average class accuracies near 80%, while the classes of secondary vegetation and residential showed accuracies of 43% and 75% respectively (figures 12 and

13). The lower class accuracy of secondary vegetation was related to commission of secondary vegetation into the class of exposed soil.

Compared to the Sentinel-1 classification overall accuracies of 56% and 38%, the Sentinel-2 classification image had notably higher overall accuracy. However, Sentinel-2 class accuracies across the forest, exposed soil, and secondary vegetation were similar to those seen in Sentinel-1. The primary differences between the class accuracies across Sentinel-1 and Sentinel-2 were observed in the classes water and residential. The Sentinel-2 class accuracies for residential and water increased by nearly 40-45% from the accuracies observed by the Sentinel-1 classes of residential and water. This highlights a significantly larger capability by Sentinel-2 for separating these classes from forest, exposed soil, and secondary vegetation.

Overall, the Sentinel-2 derived classification maps had high accuracies, which were particularly pronounced in the classes of residential and water through reductions in commission and omission errors observed by the Sentinel-1 classes of residential and water. The classes of exposed soil, forest, and secondary vegetation demonstrated similar commission errors as those observed in the Sentinel-1 classification image and of those commission errors, the largest was observed in the class of secondary vegetation, which demonstrated repeated confusion with the class of exposed soil.

4.1.3 Combined Sentinel-1 and Sentinel-2

The combination of Sentinel-1 and -2 had overall map accuracies of 78% and 72% for case studies 1 and 2 respectively (figure 11). These land cover maps had higher overall map accuracies compared to the both Sentinel-1 and Sentinel-2 derived classification maps (figure 8). Across case studies, all classes experienced increases in accuracy compared to those observed in either Sentinel-1 or Sentinel-2 classification images. These higher class accuracies translated into lower errors of commission and omission, particularly in the secondary vegetation class (table 3). In the Sentinel-2 classification image, secondary vegetation had a commission error of 58% which primarily contributed to omission

error in the Sentinel-2 class of exposed soil (table 3). Similarly, in the Sentinel-1 classification image, secondary vegetation had a commission error of 60% primarily contributing to omission error in the Sentinel-1 class of forest. Through combining the Sentinel-1 and Sentinel-2, the overall secondary vegetation commission error was reduced to 45%, with 30% of this error being related to omissions in exposed soil and 12% being related to omissions in forest. The confusion due to the misclassification of secondary vegetation by either Sentinel-1 and Sentinel-2 individually, was mitigated through the combination of the two, utilizing both spectral and backscatter class signatures. Thus, combining Sentinel-1 VV and VH polarization backscatter with Sentinel-2 multispectral bands resulted in the greatest class and map accuracies and reduced class through disaggregating secondary vegetation from Sentinel-2 exposed soil, and Sentinel-1 forest.

4.3.3 Cross Tabulation of Sentinel-1, Sentinel-2, and Combined Sentinel-1 and -2 Classification Images

Despite differences in map accuracy, the overall map agreement (as derived from image cross tabulation across Sentinel-1, Sentinel-2, and the combined Sentinel-1 and -2) was high. The Sentinel-1 classifications agreed with 83-95% of the class assignments from both the Sentinel-2 classifications and the combined Sentinel-1 and -2 classifications, across case studies (figures 14 – 19). The Sentinel-2 classification and the combined Sentinel-1 and -2 classifications agreed upon 95-99% of the class assignments across case studies.

The largest sources of the 5-17% disagreements, between the Sentinel-1 classifications and the other classifications derived from Sentinel-2 and combined Sentinel-1 and -2, were between the classes of forest and exposed soil. The classification based on Sentinel-1 VV and VH polarization bands presented a smaller amount of exposed soil areas, with locations identified as forest in Sentinel-1, classified as Exposed Soil in Sentinel-2 and the combined Sentinel-1 and -2. These areas of disagreement were typically observed in homogenous areas of low Sentinel-1 VV and VH backscatter. The second

largest component of disagreement, was seen between the Sentinel-1 class of forest and the Sentinel-2 and combined Sentinel-1 and -2 classes of secondary vegetation.

Overall, the disagreement between Sentinel-2 and the combined Sentinel-1 and -2 was low, ranging from 1-4%. The low disagreement between these classifications, included the Sentinel-2 class of forest being disaggregated into the classes of exposed soil, secondary vegetation, and water in the Sentinel-1 and -2 classification images. The combined Sentinel-1 and -2 class of exposed soil was also extracted from the Sentinel-2 class of secondary vegetation.

5.1 Discussion:

Overall, the mapping efficacy, as characterized by map and class accuracies, of Sentinel-1, Sentinel-2, and Sentinel-1 and -2 varied across case studies but demonstrated the potential for Sentinel-1 to delineate rough and smooth classes, Sentinel-2 to capture spectrally dissimilar classes, and for the combination of Sentinel-1 and -2 to draw from both class roughness and multispectral qualities for image classification.

The poor Sentinel-1 backscatter signature separability of classes with similar surficial roughness resulted in high commission in the residential, secondary vegetation, and water classes, and high omission in the forest and exposed soil classes. These high commission and omission errors were not as prevalent in Sentinel-2. Sentinel-2 showed high map accuracy across all classes, but showed errors of commission in the secondary vegetation class relating to omission in the class of exposed soil. Combining Sentinel-1 and -2 created a classification image that benefited from the high multispectral signature separability of the classes of residential and water and from the high backscatter signature separability between the classes of secondary vegetation and exposed soil. Thus, the overall and class accuracies were highest in the combined classification map that utilized both Sentinel-1 and -2.

Across images, there was nearly 85 – 95% similarity between the Sentinel-1 images and the Sentinel-2 and combined Sentinel-1 and -2 images. The similarity between the Sentinel-2 images and the combined Sentinel-1 and -2 images ranged from 95 – 99%. In case study 1, the majority of image disagreement is in the disaggregation of the Sentinel-1 forest class into the Sentinel-2 classes of residential, secondary vegetation, and exposed soil. The majority of disagreements between the Sentinel-2 images and the combined Sentinel-1 and -2 images is seen in the class of secondary vegetation, where the Sentinel-2 class of secondary vegetation is separated into the Sentinel-1 and -2 class of exposed soil. This disagreement between Sentinel-2 and the combined Sentinel-1 and -2 suggests that, given the increase in class accuracy from the Sentinel-2 secondary vegetation class to the Sentinel-1 and -2 secondary vegetation class, integrating backscatter and multispectral signatures aids in the delineation of secondary vegetation from exposed soil.

The speckled distribution of the Sentinel-1 exposed soil class in the Sentinel-2 class of forest, as well as the disagreement between the Sentinel-2 class of exposed soil and Sentinel-1 class of forest, describes classification disagreement likely due to SAR speckling artifacts. The apparent mischaracterization of the Sentinel-1 class of exposed soil (and forest) is likely an artifact of the constructive and destructive interference that defines homogenous land covers in SAR imagery (Smith, 2012). In this case, the scattering prevalent in homogenous areas results in highly heterogeneous backscatter values, ranging from high intensity to low intensity (figure 1). While speckle filtering mitigates this property of SAR images, the effect is not eliminated altogether, and thus, in study confusion was introduced between classes that are separated based upon high and low backscatter values (Smith, 2012).

This study adds to the body of work evaluating Sentinel-1 and Sentinel-2. Clerici et al. (2017) observed, in a Colombian case study, map accuracies of random forest classifications for Sentinel-1 texture bands, Sentinel-2, and combined Sentinel-1 and-2 as 20.12%, 48.1%, and 55.5% respectively.

While from a differing region and using an alternate classification procedure (which had incorporated texture bands of VV and VH as well as segmented training sites through eCognition), the classification capabilities of Sentinel-1 and Sentinel-2 followed the same hierarchy as observed in this study, with the integration of Sentinel-1 and -2 showing the highest overall accuracy followed by Sentinel-2 and then Sentinel-1. In their work, the investigators were separating the classes of forests, secondary vegetation/shrubs, cropland, water, pastureland, and built areas. The much lower classification accuracies could be a result of the different classes evaluated, differences in the classification procedures, or in non-stationarity across regions. It is likely that More case studies should be performed to further characterize the performance of both Sentinel-1 and Sentinel-2 for land cover classification.

In this work, the Sentinel-1 classification accuracies across both case studies were lower than the reported Sentinel-1 classification accuracies by Abdikan et al. (2017). Abdikan et al. (2017) evaluated the classification potential of Sentinel-1 VV and VH polarization backscatter bands in Turkey. Abdikan et al. (2017) showed overall map accuracies near 90% using a support vector machine classification of the classes urban, water, forest, bare land, and agriculture. The large difference between the observed Sentinel-1 classification accuracy in this study compared to the study conducted by Abdikan et al. (2017) could be due to differences in scale, class sampling procedure, classification method, and or non-stationarity of sensor performance.

This study argues, that Sentinel-1 could be useful for land cover mapping where weather conditions prevent routine image acquisition and where class multispectral separability requires additional information for delineating classes through scattering qualities, such as separating secondary vegetation from bare ground. These benefits are contrasted against the extensive data preprocessing requirements, the large data storage requirements, and processing time of SAR data. Compared to the preprocessing requirements of optical imagery, preprocessing SAR is time consuming and computationally expensive. Given these requirements for conducting SAR analysis, further work should

evaluate the effect of combining temporally neighboring Sentinel-1 images to determine how map accuracies, specifically error due to the random speckle in homogenous land cover types, fluctuate with the addition of backscatter information. Through characterizing how land cover classification accuracies increase with increasing SAR images, an optimal number of images can be identified to maximize accuracy while mitigating processing requirements.

Sentinel-2 demonstrated high accuracies for capturing high resolution land cover. Even with a subset of the bands equipped on the MSI sensor, high map accuracies were achieved for fundamental land cover classes of forest, exposed soil, water, residential, and secondary vegetation. Combined with the relative ease of acquiring and preprocessing Sentinel-2 imagery through the SNAP software, highlights the operational potential of the sensor for future land change monitoring projects, including REDD+.

Together, Sentinel-1 and -2 are shown to benefit from their respective strengths, thereby increasing overall map accuracy through class multispectral and backscatter characterization. The most pronounced effect of combining the two sensors was the separation of the Sentinel-2 secondary vegetation class into the combined Sentinel-1 and -2 exposed soil class. This highlights potential for extraction of sparsely vegetated land cover from bare ground. Further work should explore the limits to which the combination of Sentinel-1 and -2 benefits classifying a wider range of land cover types.

6. 1 Conclusion:

This study used Sentinel-1 and Sentinel-2 both individually and in tandem to create six land cover classification maps along the border of the Pando department of Bolivia to evaluate their respective classification capabilities. Using a random forest classifier to produce these images and evaluating the end products through both general confusion matrices, Sentinel-1 proved useful to generate simple land cover classifications based on landscape surficial roughness. The integration of

Sentinel-1 with Sentinel-2, increased map accuracy through characterizing classes through multispectral and backscatter signatures. The most appropriate use of a single date non-textural classification of Sentinel-1 backscatter values is over a landscape which has classes that are distinct in surficial roughness, as it was predominantly between similarly textured classes that Sentinel-1 demonstrated the greatest confusion. For a project with the goal of delineating forested areas from non-forested areas, Sentinel-1 may be of significant use to classify landscapes often obscured by cloud cover and to act as additional ancillary information to decrease overall map error.

Figures:

Table 1 Sensor Specifications for Sentinel-1 and Sentinel-2, the sensors evaluated and used in this study.

Sensor	Spectral Resolution (bands)	Temporal Resolution (days)	Spatial Resolution (m)
Sentinel-1	C-Band	12	5 by 20
Sentinel-2	13 bands from VNIR to SWIR	5	10, 20, and 60

Table 2: Data Products and Parameters for the products used in this study.

Sensor	Sentinel-2A	Sentinel-1A
Name	S2A_MSIL1C_20180904T144731_N0206_R139_T19LFJ_20180904T182517	S1A_IW_GRDH_1SDV_20180906T100603_2018_0906T100630_023576_029175_6F5C
Acquisition Date	September 4, 2018	September 6, 2018
Product Type	S2 MSI Level-1C	GRD
Bands	490 nm, 560 nm, 665 nm, 842 nm	VV and VH
Mode		IW
Pass		Descending
Orbit		23576
Track		54

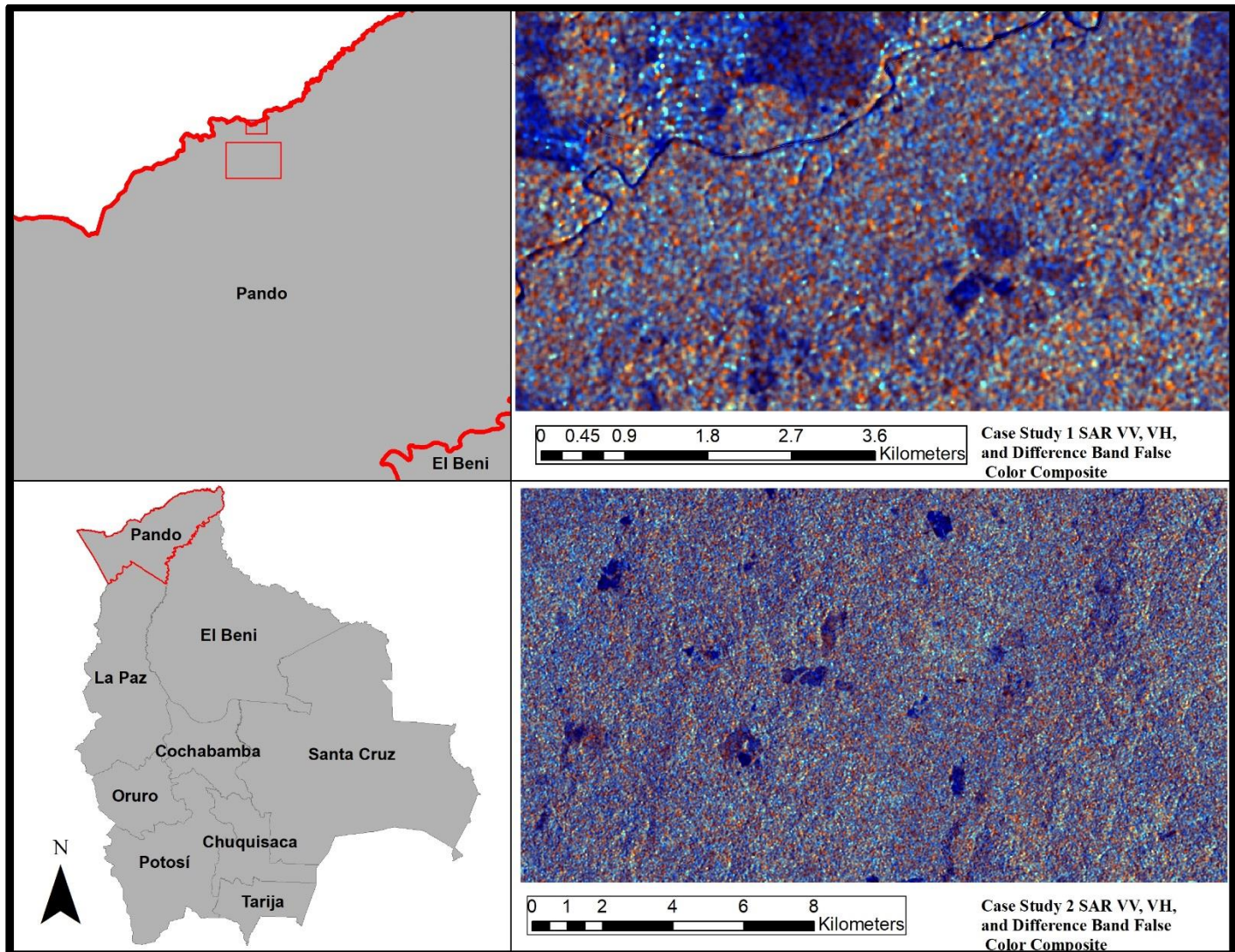


Figure 1: Study area map depicting the two case study locations, through Sentinel-1 VV, VH, and VV/VH RGB false color composites, in the Pando Department of Bolivia in the Northern region of the country sharing a border with Brazil. Forest is captured through the primary speckling depicted throughout the both images. Exposed soil and bare ground are captured in dark blue patches throughout the scene. Secondary vegetation is intermixed with subdued red and blue colorations. Water appears dark blue while some of the brightest pixels capture Residential areas as seen in Case Study 1 where there is a cluster of bright white pixels in the North central area of the scene.

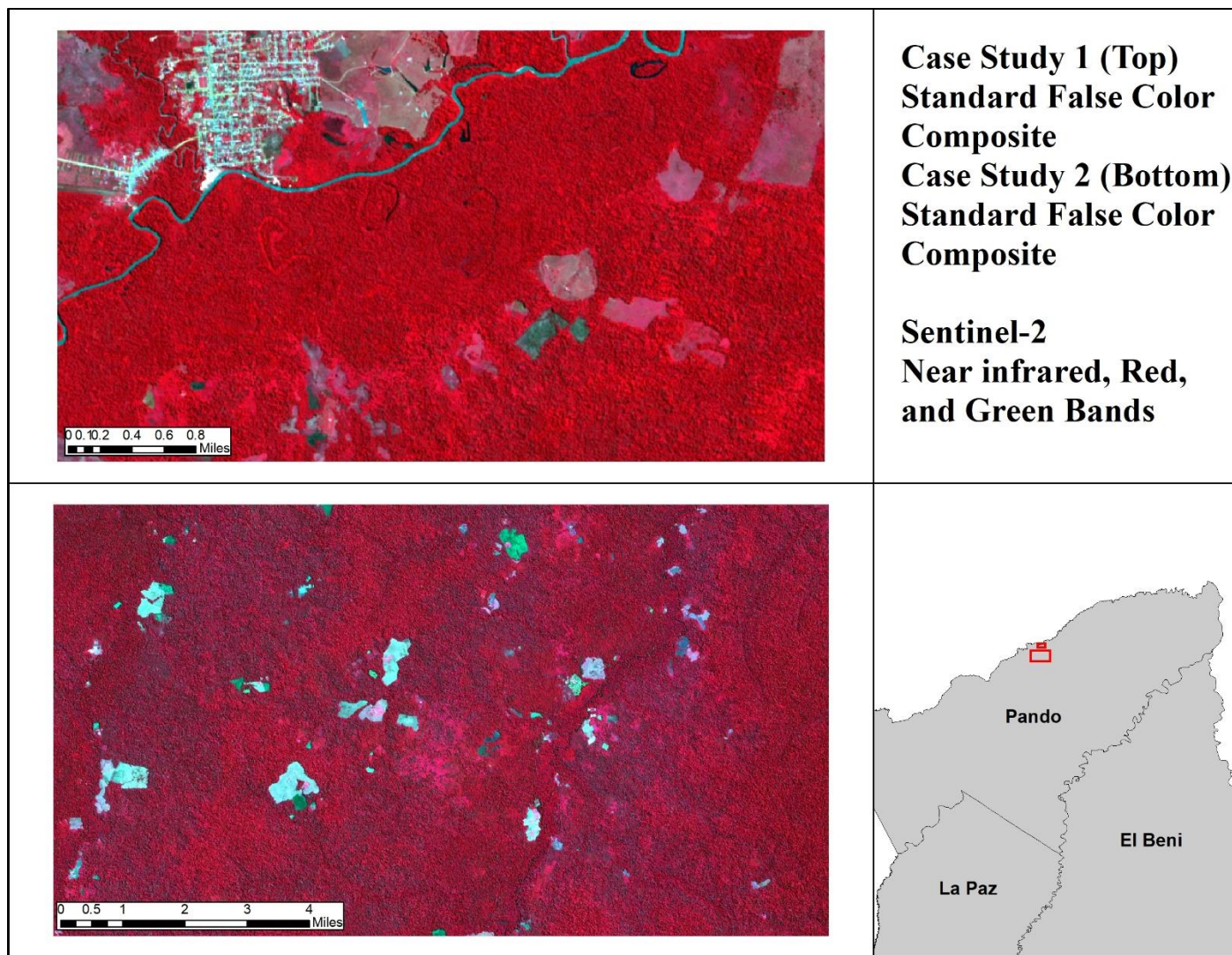


Figure 2: Depicted above are the case study locations visualized through the conventional RGB false color composite using the Sentinel-2 Red, Green, and Near infrared bands. The dense forested landscape is depicted through varying shades of red to maroon. Secondary vegetation, which is a transitional class between low lying shrubbery and overgrown grasslands appears pink to light red in coloration for both images. The residential area in the municipality captured in the north central region of case study 1 is depicted as cyan to bright white. Exposed soil varies in coloration from highly reflective bright white and blue to a deeper green and gray color. The rivers, vary in coloration from each case study. In case study 1 there is a light blue color to the river with dark gray to black stagnant water sources nearby. In Case study 2, the river is much smaller and obscured by trees but stretches from the South central region of the study area across to the Northeast section of the study area and is seen through its dark grey coloration.

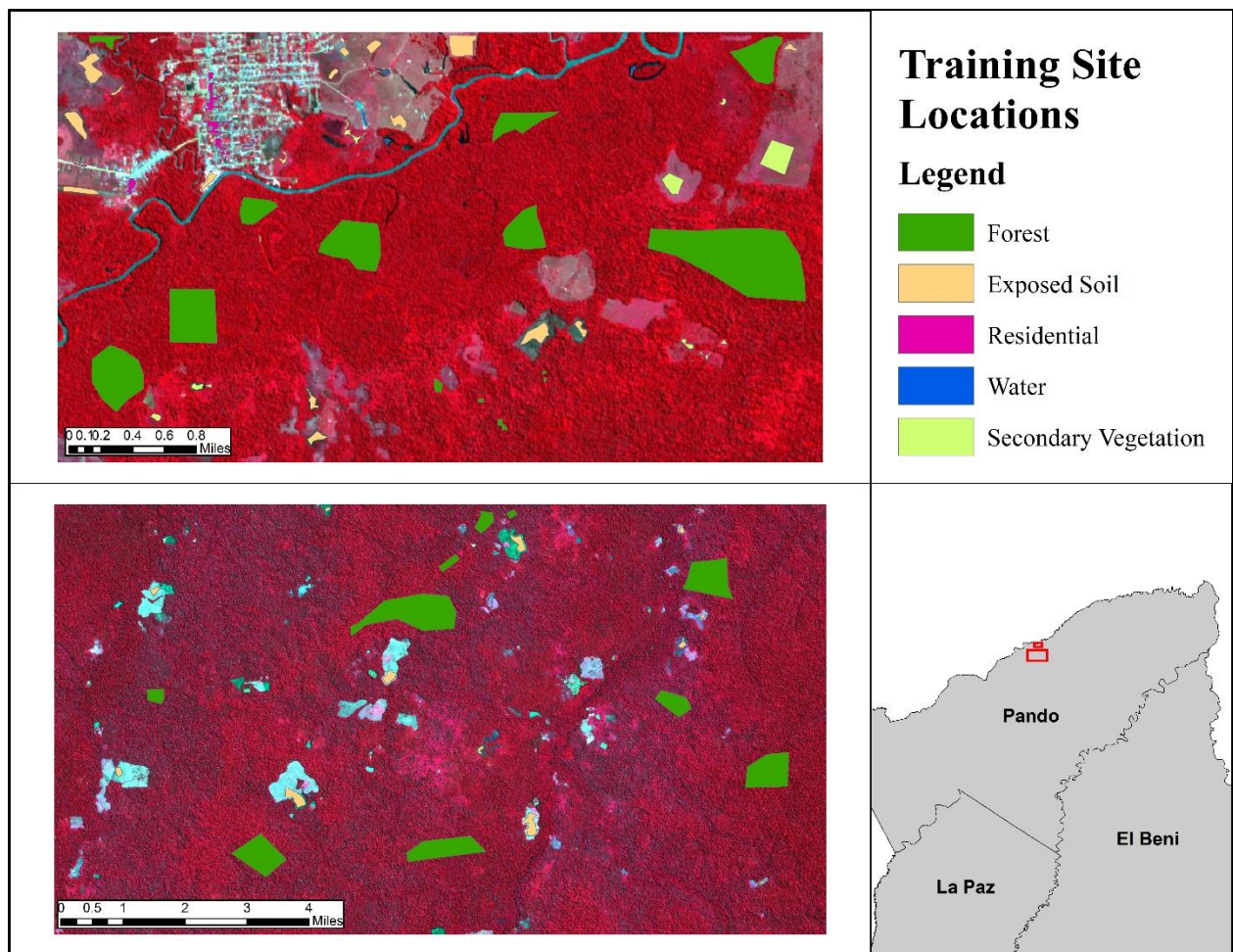


Figure 3: False Color Composites from Sentinel-2 for case study 1 and case study 2, depicting final training sites.

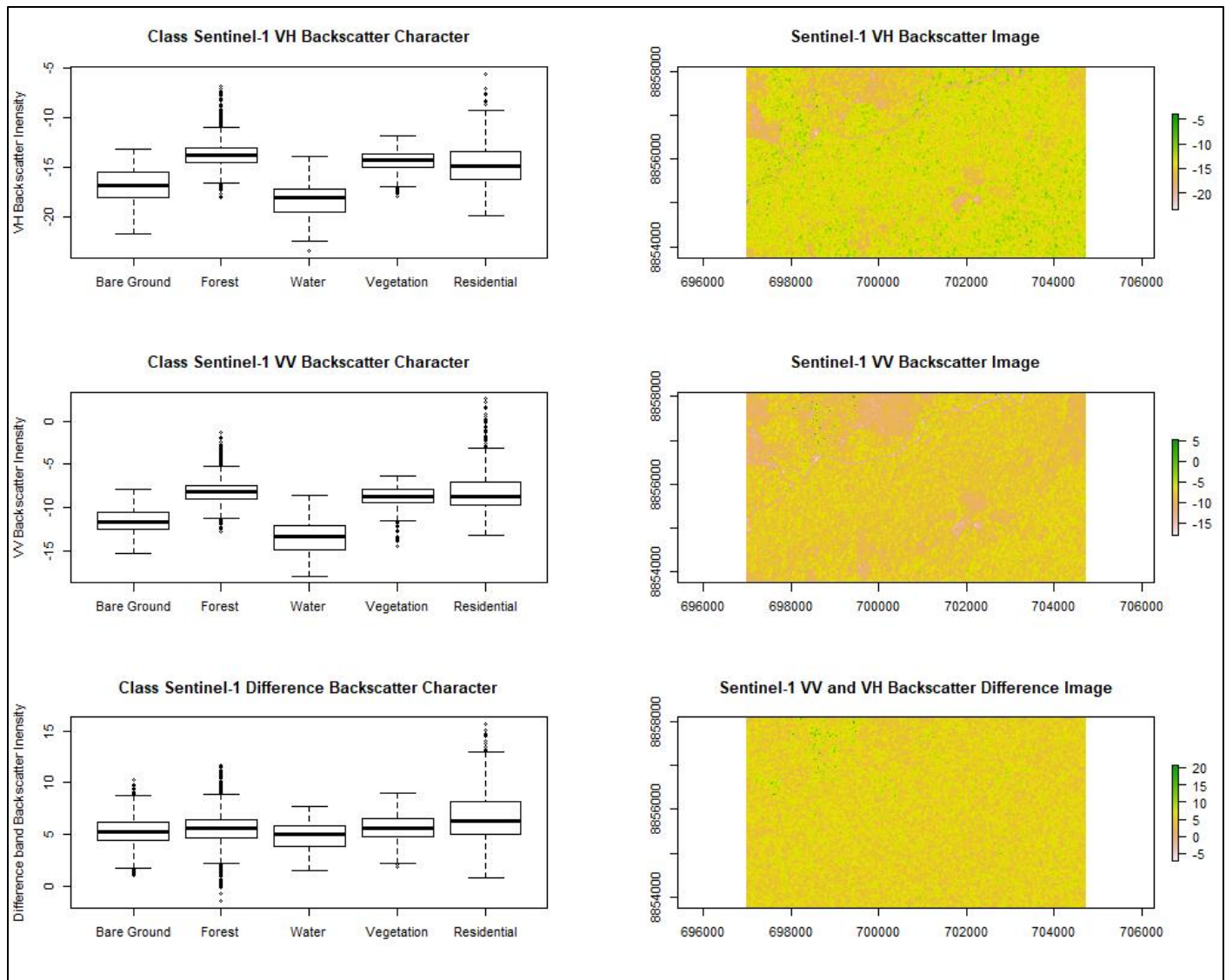


Figure 4: Sentinel-1 SAR Backscatter Values for extracted by training sites for Case Study 1. The VH, VV, and difference backscatter images visualized across the from the respective boxplots highlight the large overlap in backscatter intensity between classes of similar textures. VH backscatter values typically are seen to be lower than the VV backscatter values across all classes, but demonstrate a similar pattern of class backscatter response where Forest, Vegetation (discussed in the paper using the term 'Secondary Vegetation'), and Residential exhibit higher backscatter values on average than the bare ground and water classes.

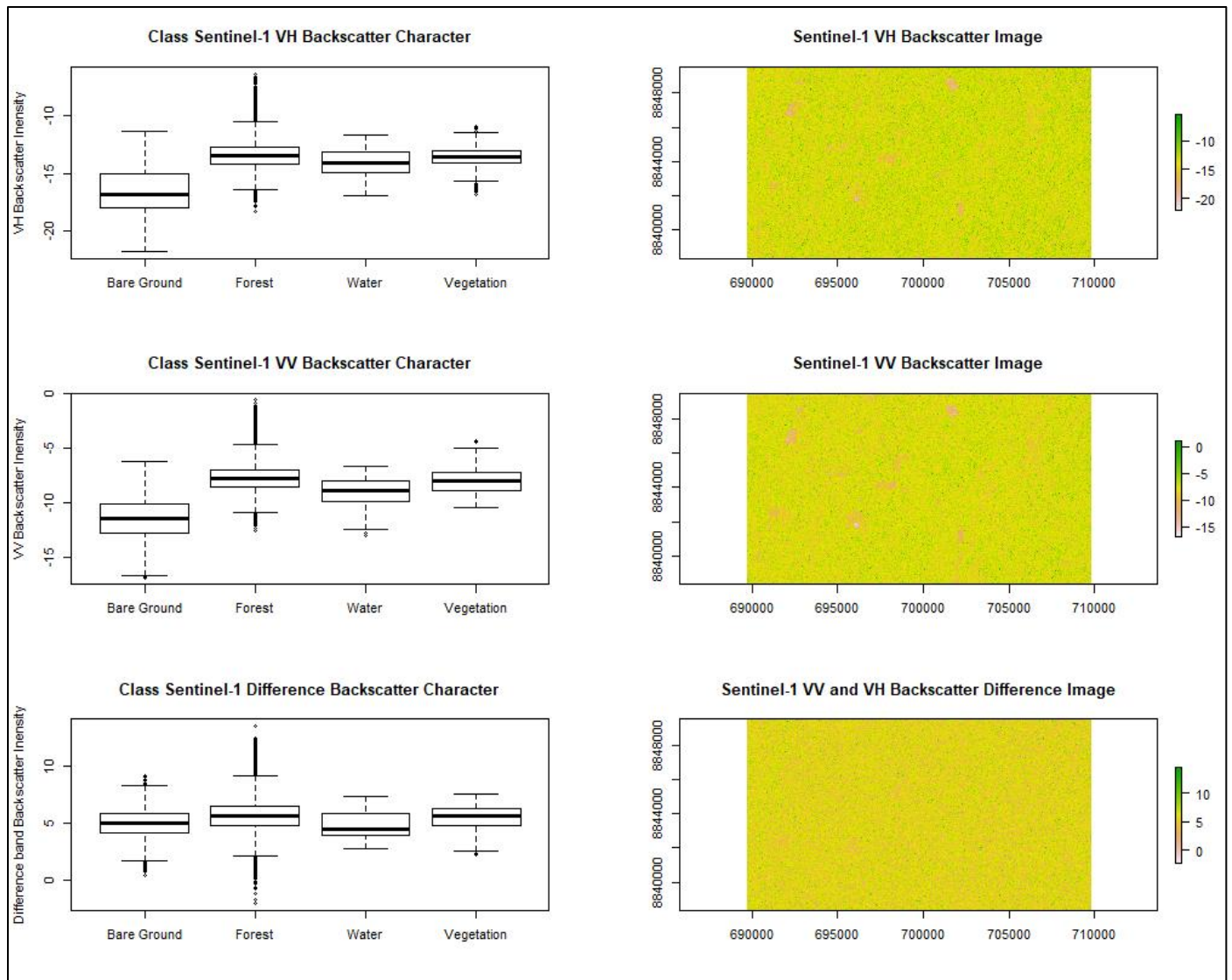


Figure 5: Sentinel-1 Backscatter values for each class extracted by the training sites depicted above. Just as in case study 1, the VH, VV, and difference backscatter images visualized across the from the respective boxplots highlight the large overlap in backscatter intensity between classes of similar textures, with the exception of the difference backscatter band and the Water class. The water class depicts an average class backscatter intensity equal to Forest and Secondary Vegetation (labeled vegetation).

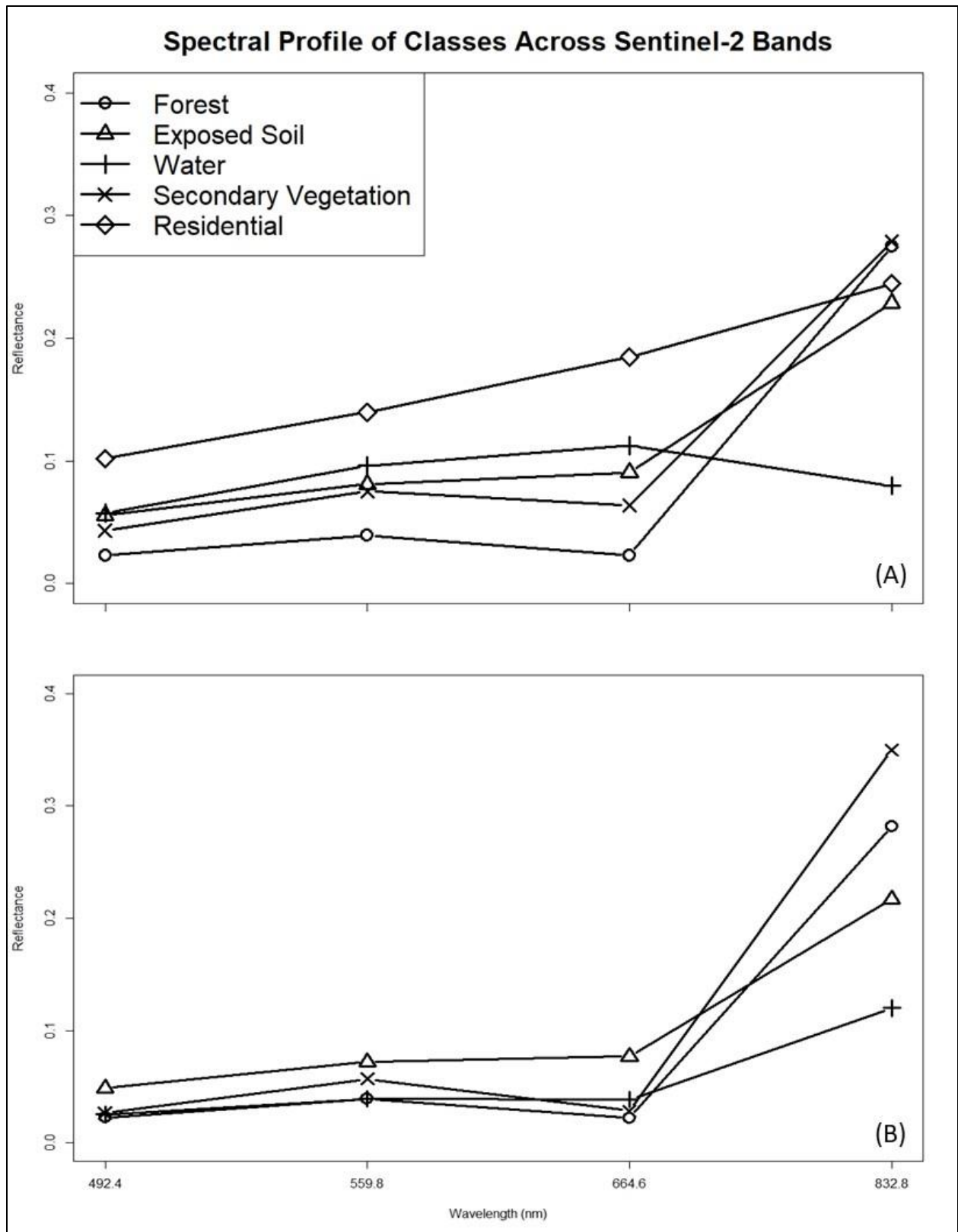


Figure 6: Sentinel-2 mean reflectance values across the blue (492.4 nm), green (559.8 nm), red (664.6 nm), and near infrared (832.8 nm) bands for each class extracted by the training sites in case studies 1 and 2, shown in (A) and (B) respectively.

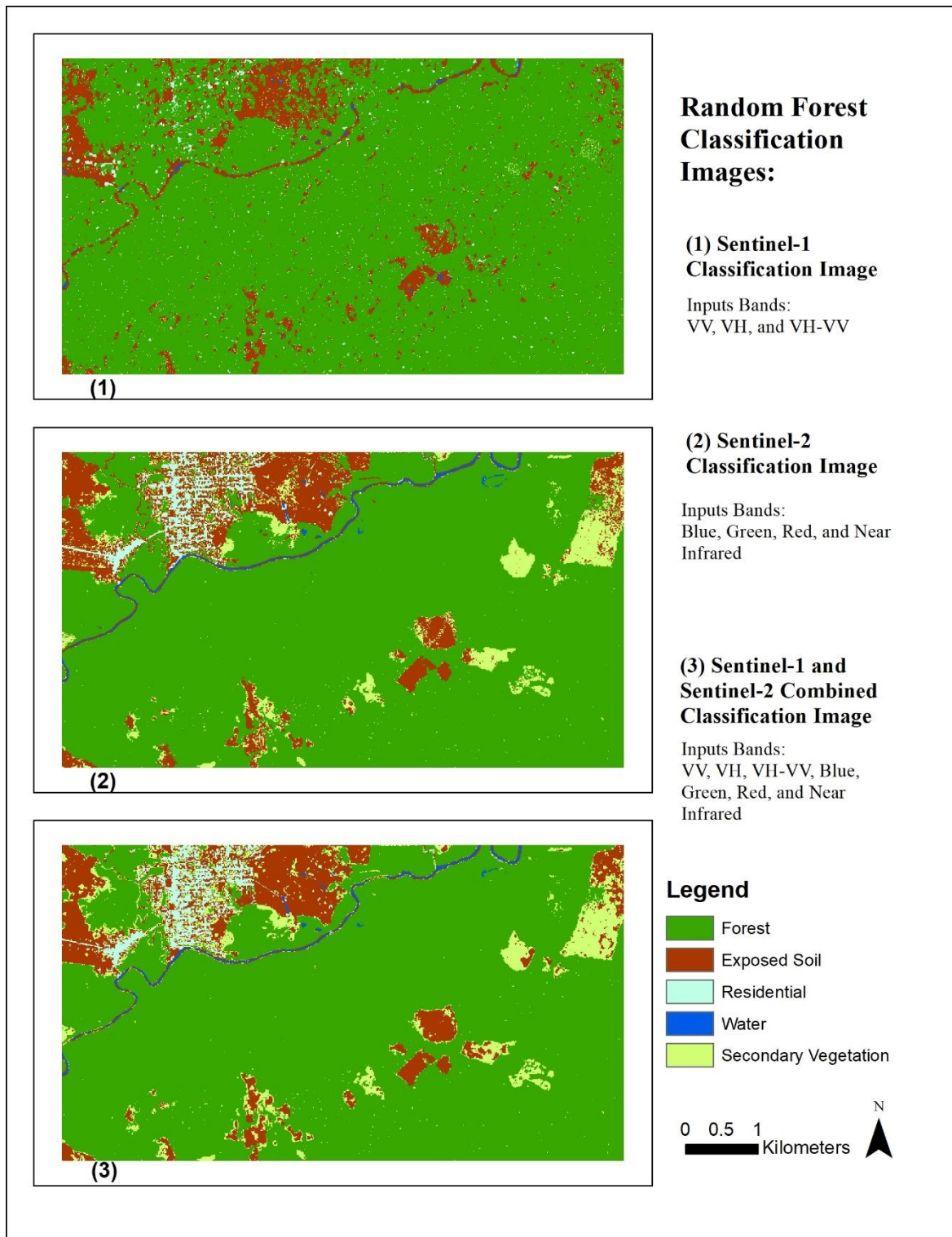


Figure 7: Random Forest Classification images for: (1) Sentinel-1 backscatter bands and backscatter difference band, (2) Sentinel-2 visible and near infrared optical bands, and (3) the combined Sentinel-1 backscatter and Sentinel-2 optical bands in Case Study 1. Individual random forest models were trained and used to predict land cover for each classification separately. The training incorporated every pixel provided through the training data and used 1000 decision trees.

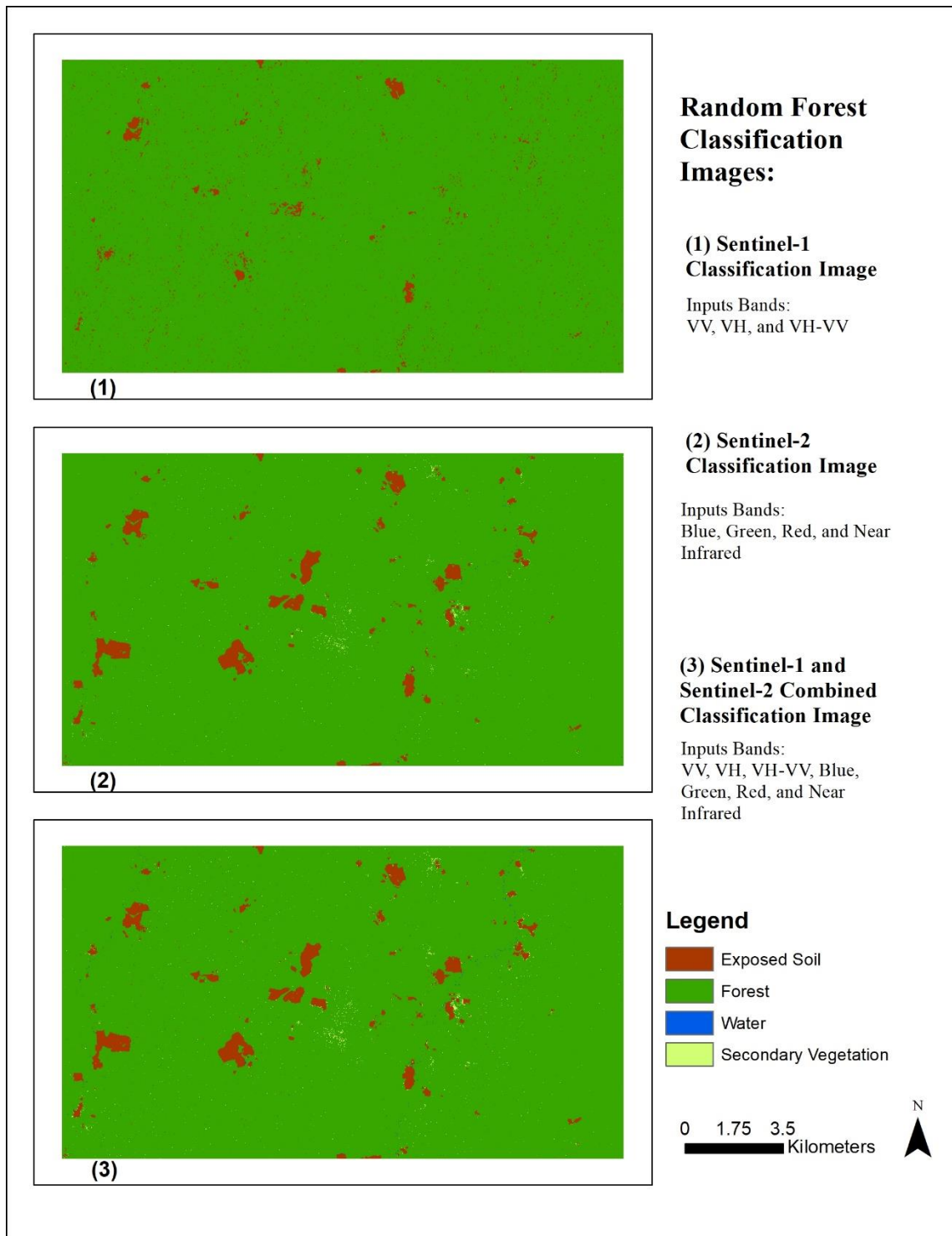


Figure 8: Random Forest Classification images for: (1) Sentinel-1 backscatter bands and backscatter difference band, (2) Sentinel-2 visible and near infrared optical bands, and (3) the combined Sentinel-1 backscatter and Sentinel-2 optical bands in Case Study 2. Identical to case study 1, Individual random forest models were trained and used to predict land cover for each classification separately using 1000 decision trees.

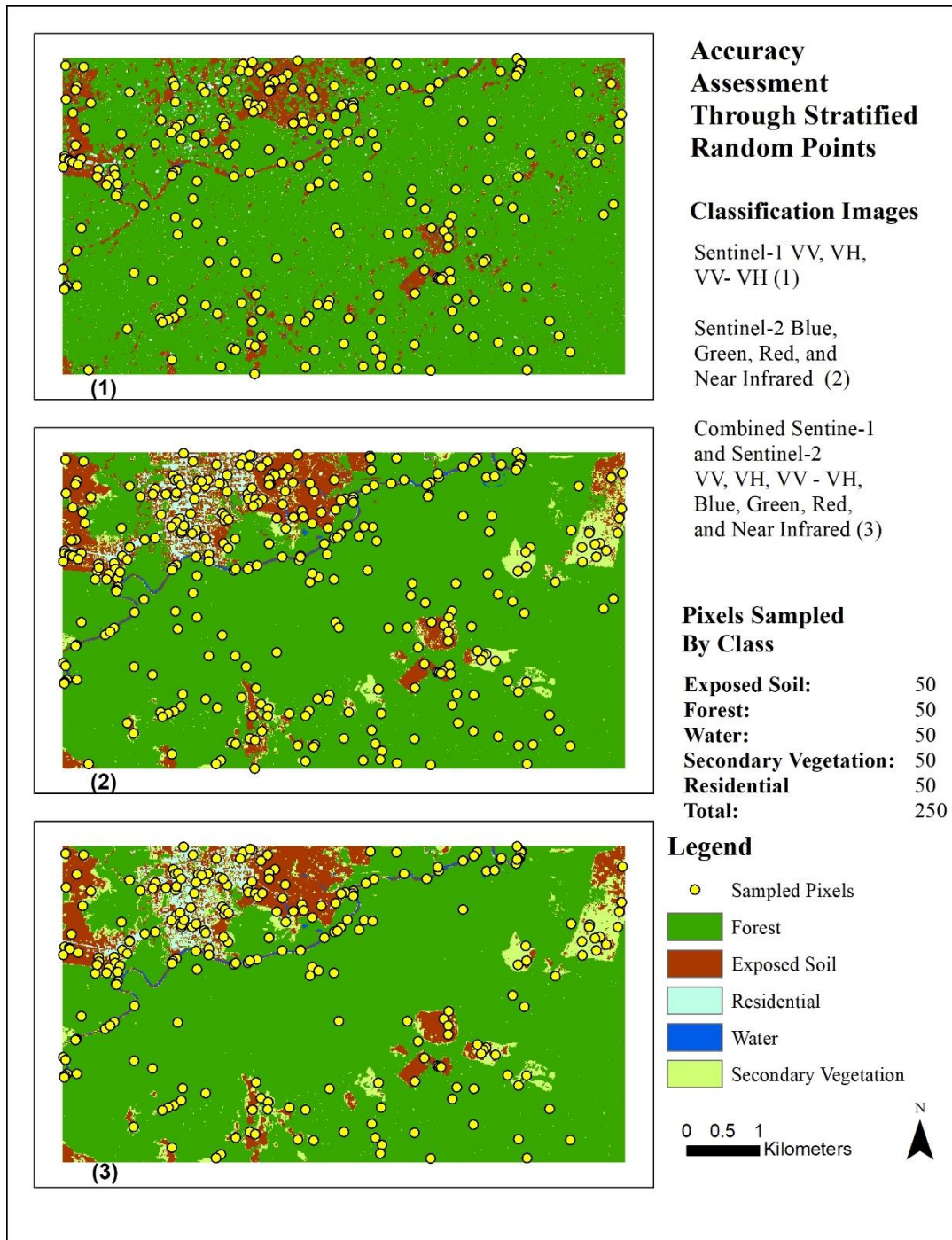


Figure 9: Case 1 Accuracy Assessment points for each classification image. Due to spatial differences between the classes captured in the Sentinel-1 image vs the Sentinel-2 and combined Sentinel product, each accuracy assessment was independently created and evaluated.

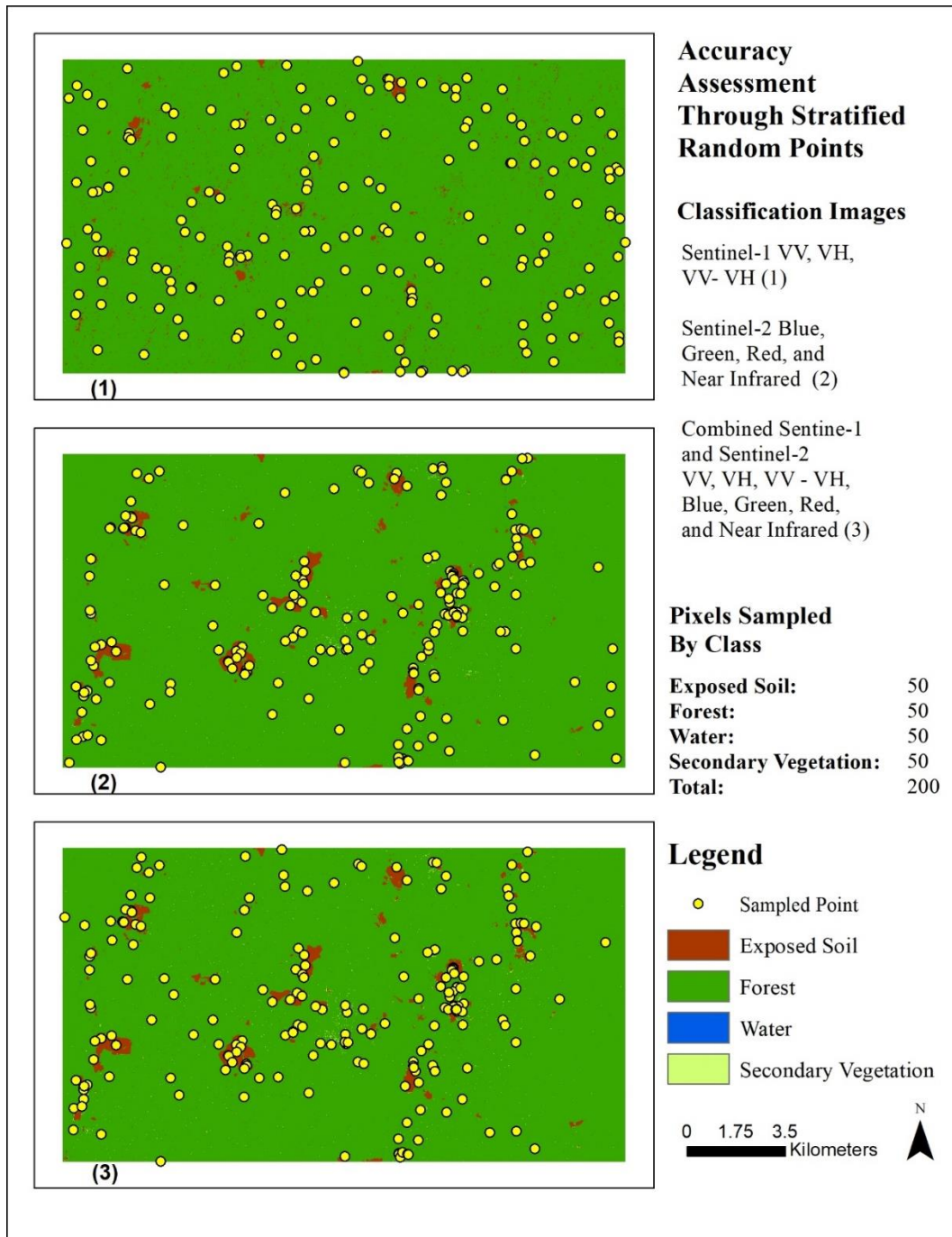


Figure 10: Case study 2 accuracy assessment points for each classification image. While the spatial allocation of classes remained largely different between the Sentinel-1 classification image and the other two classifications, the Sentinel-2 and combined Sentinel image were coincident enough in class allocation to use the same stratified sample points for each image while preserving the equal class sampling.

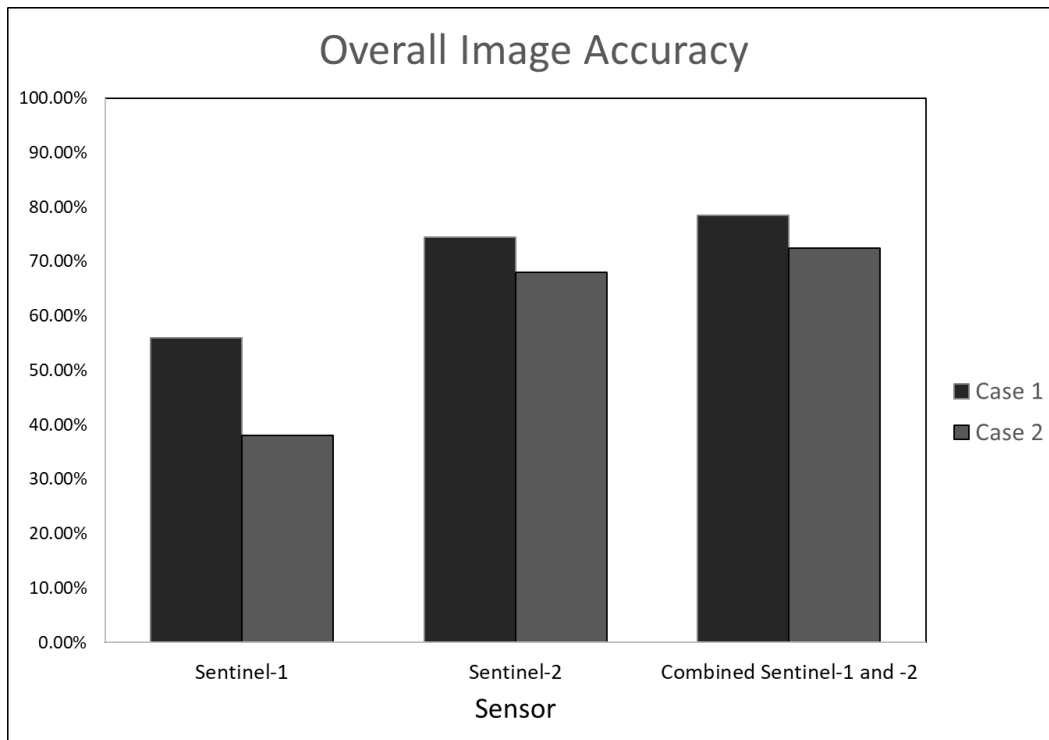


Figure 11: Case 1 and 2 overall accuracies calculated through a confusion matrix of the stratified randomly sampled points possessing ground truth class information and classification image designations. The percent overall accuracy is a calculation of the number of points that observed the same image class and ground truth class designations divided by the total number of samples points. In both case studies, the Sentinel-1 images showed lower overall percent correct than the Sentinel-2 and combined Sentinel-1 and Sentinel-2 images.

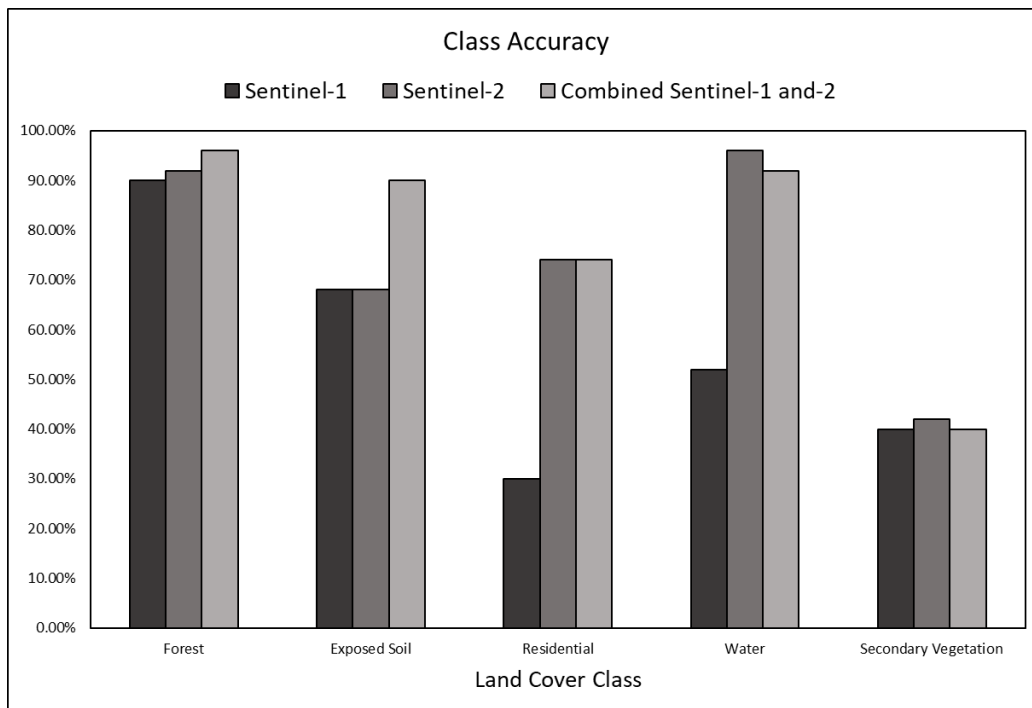


Figure 12: Case 1 class accuracies calculated through a confusion matrix of the sampled points possessing ground truth class information and classification image designations. The class accuracy is a calculation of the number of points that observed the same image class and ground truth class designations divided by the total number of samples in that class.

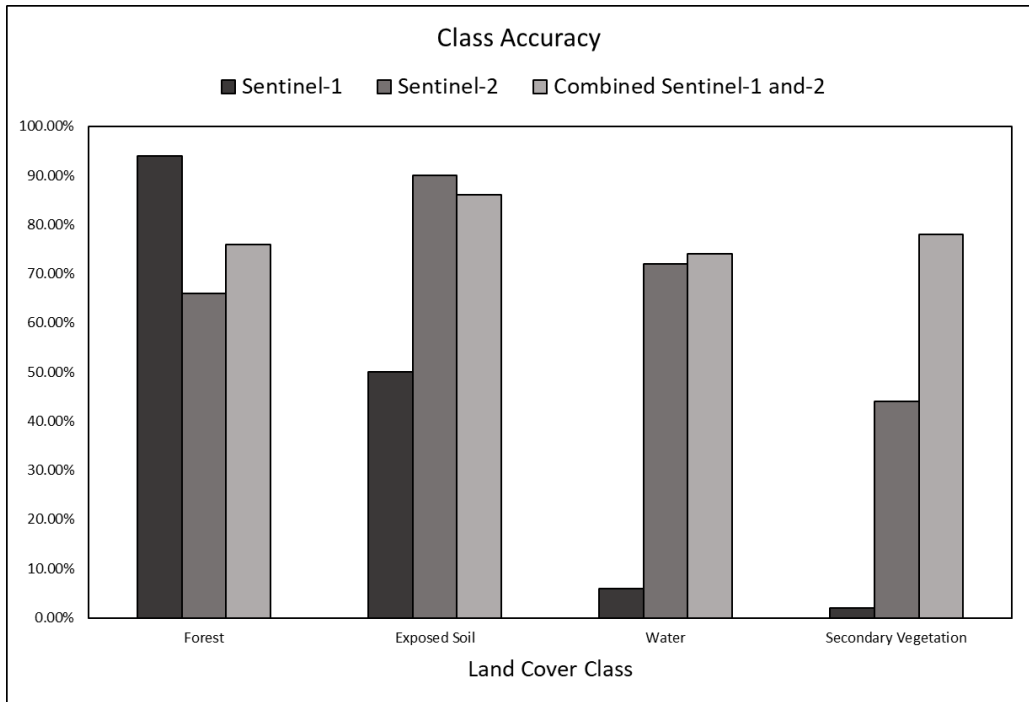


Figure 13: Case 1 class accuracies calculated through a confusion matrix of the sampled points possessing ground truth class information and classification image designations. The class accuracy is a calculation of the number of points that observed the same image class and ground truth class designations divided by the total number of samples in that class.

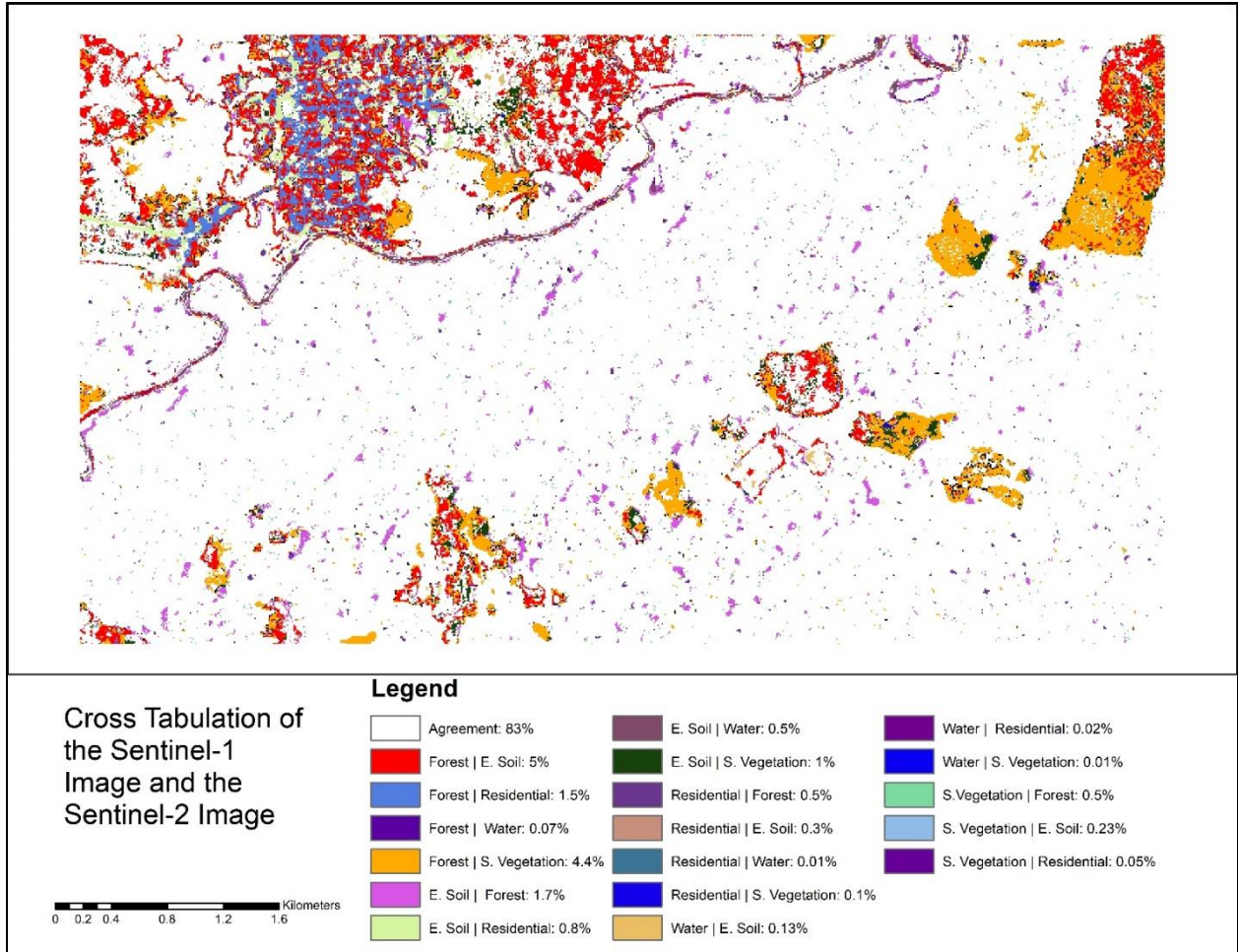


Figure 14: Cross tabulation of Sentinel-1 and Sentinel-2 Images Case 1 depicting areas of disagreement by proportion of entire image.

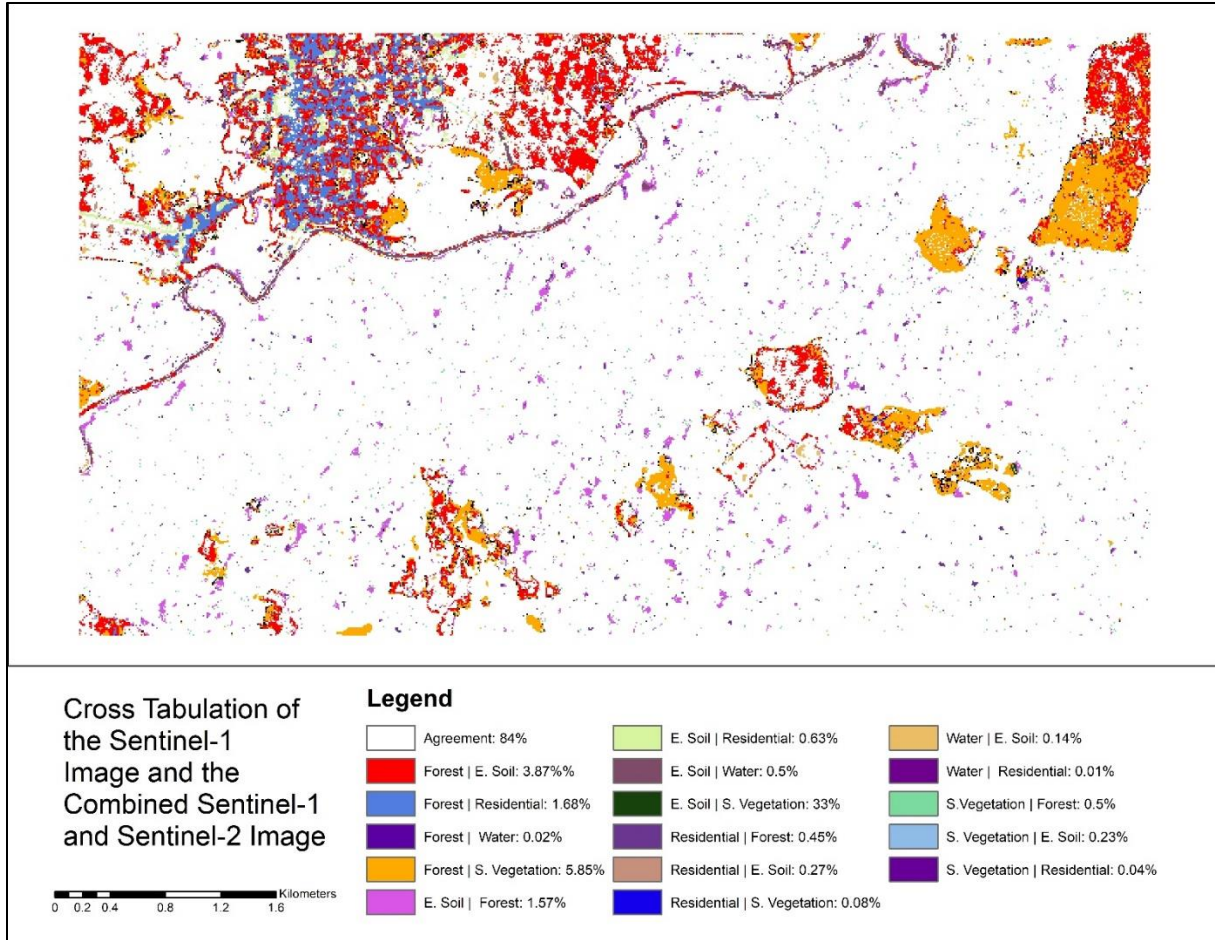


Figure 15: Cross tabulation of Sentinel-1 and combined Sentinel-1 and -2, showing areas of disagreement by proportion of Image.

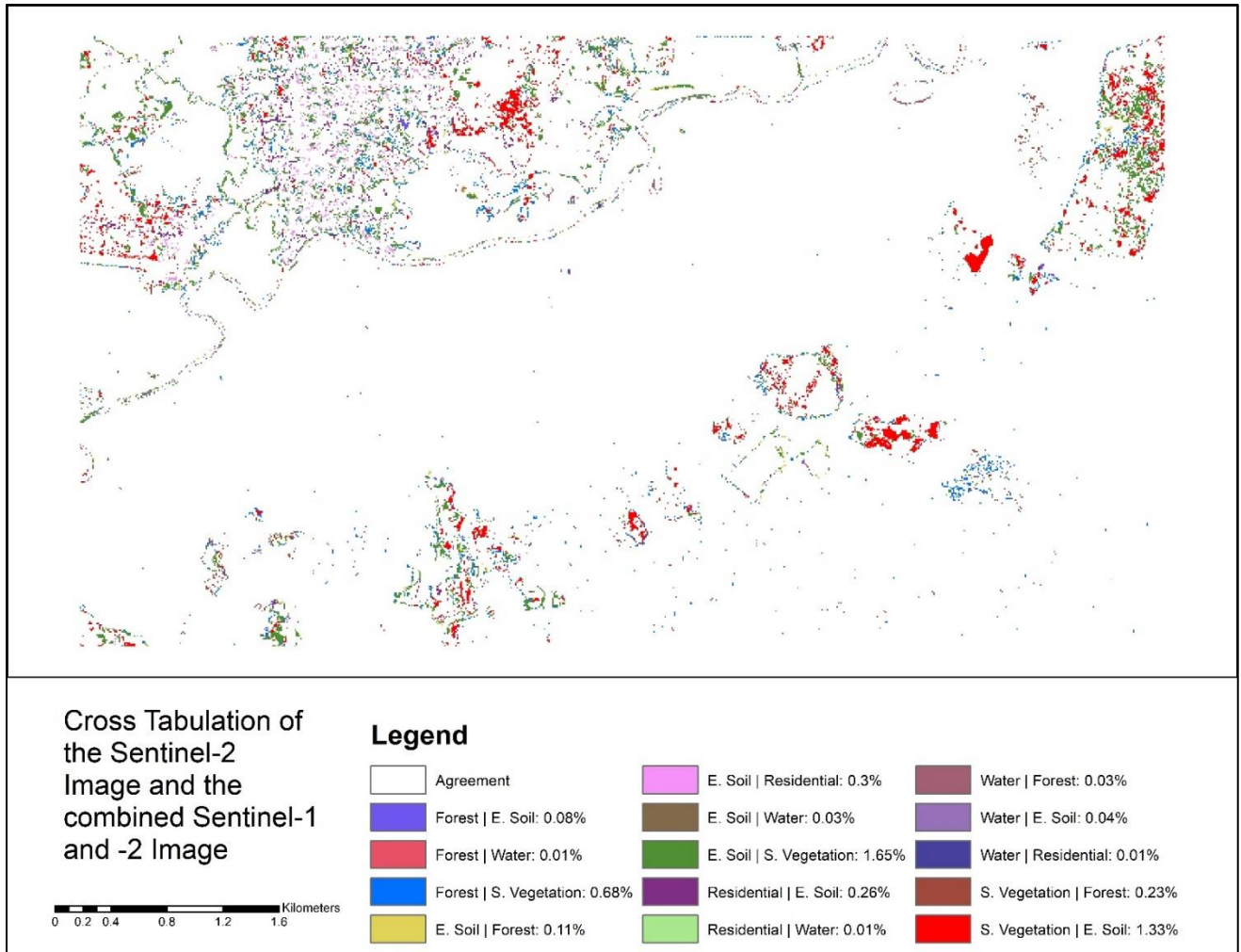


Figure 16: Cross tabulation of Sentinel-2 and combined Sentinel-1 and Sentinel-2, showing areas of disagreement by proportion of Image.

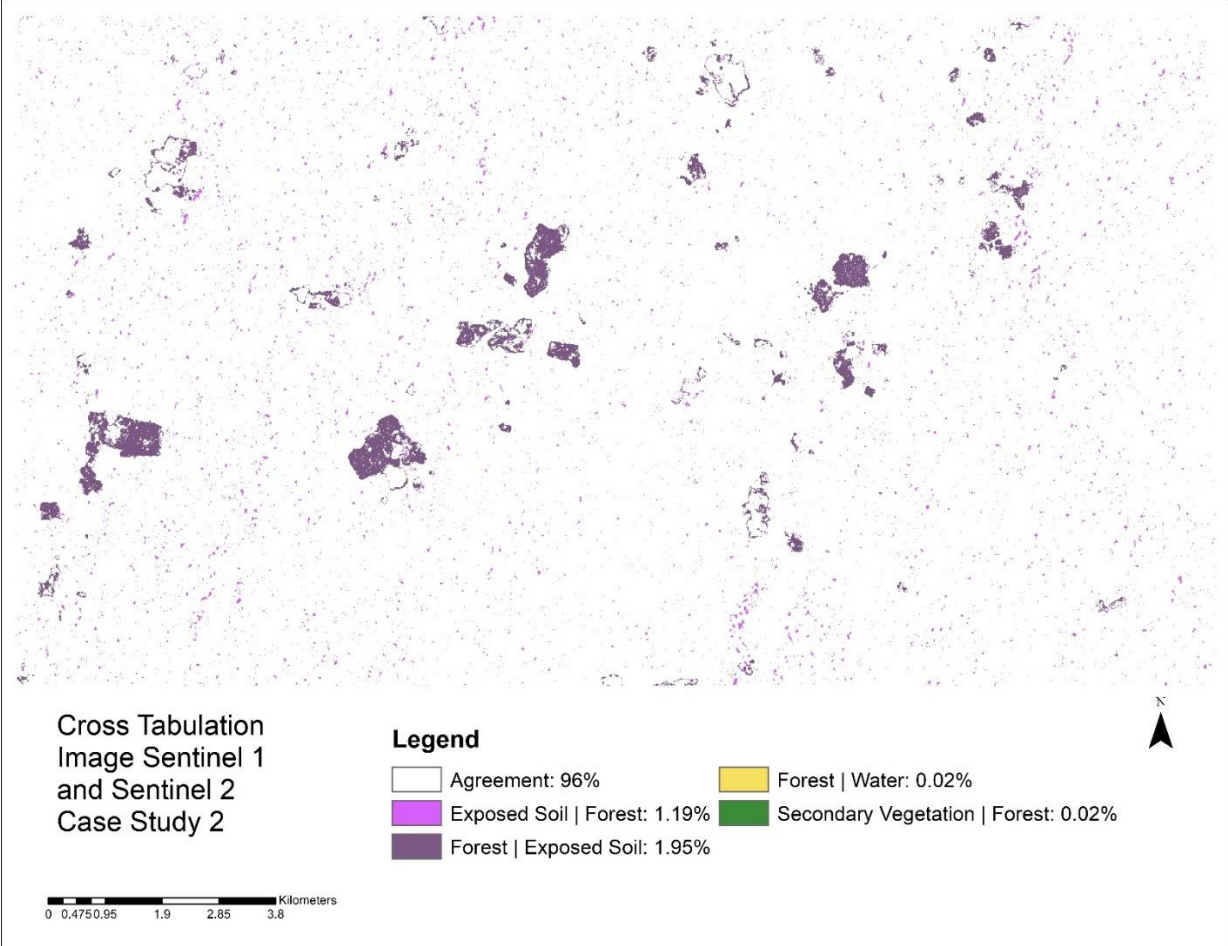


Figure 17: Cross tabulation image between Sentinel-1 and Sentinel-2 Case Study 2

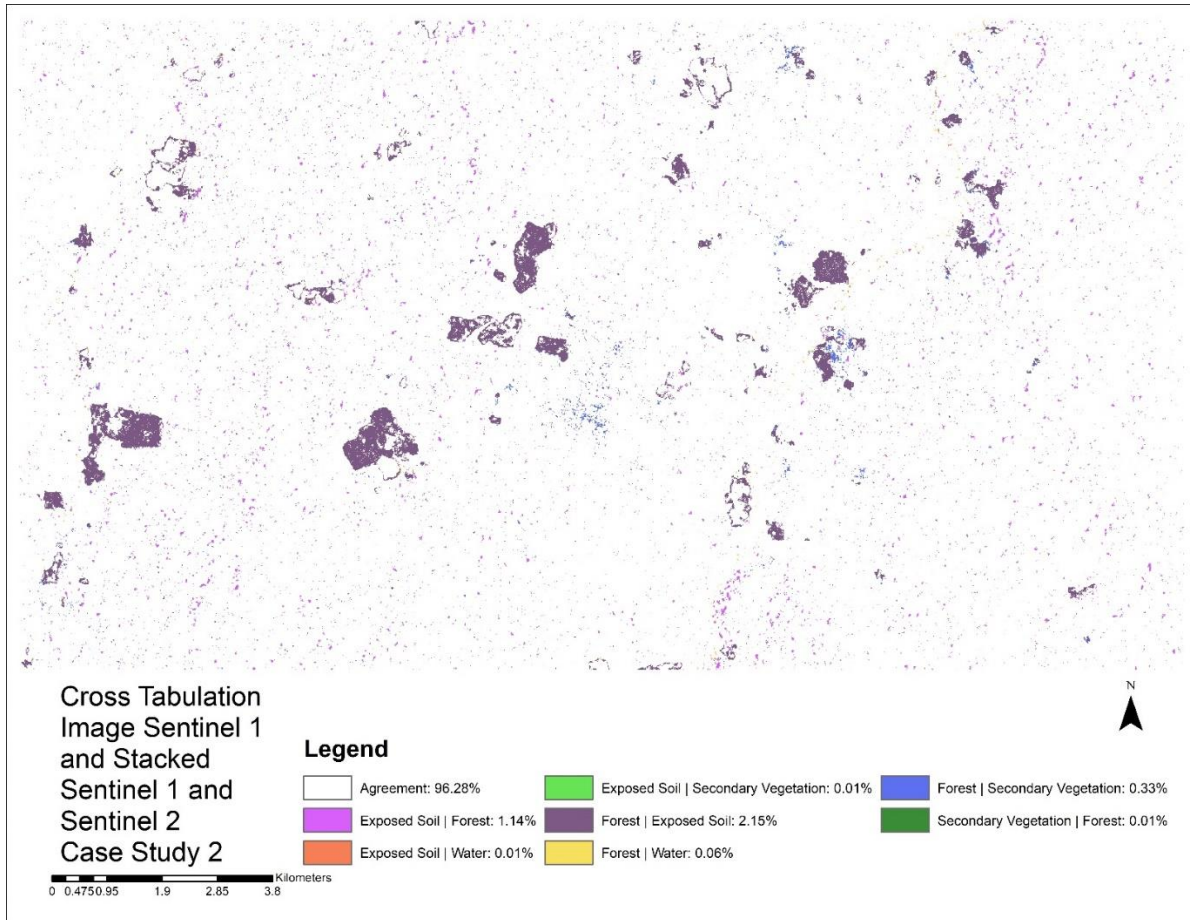


Figure 18: Cross tabulation image between Sentinel-1 and combined Sentinel-1 and -2 Case Study 2

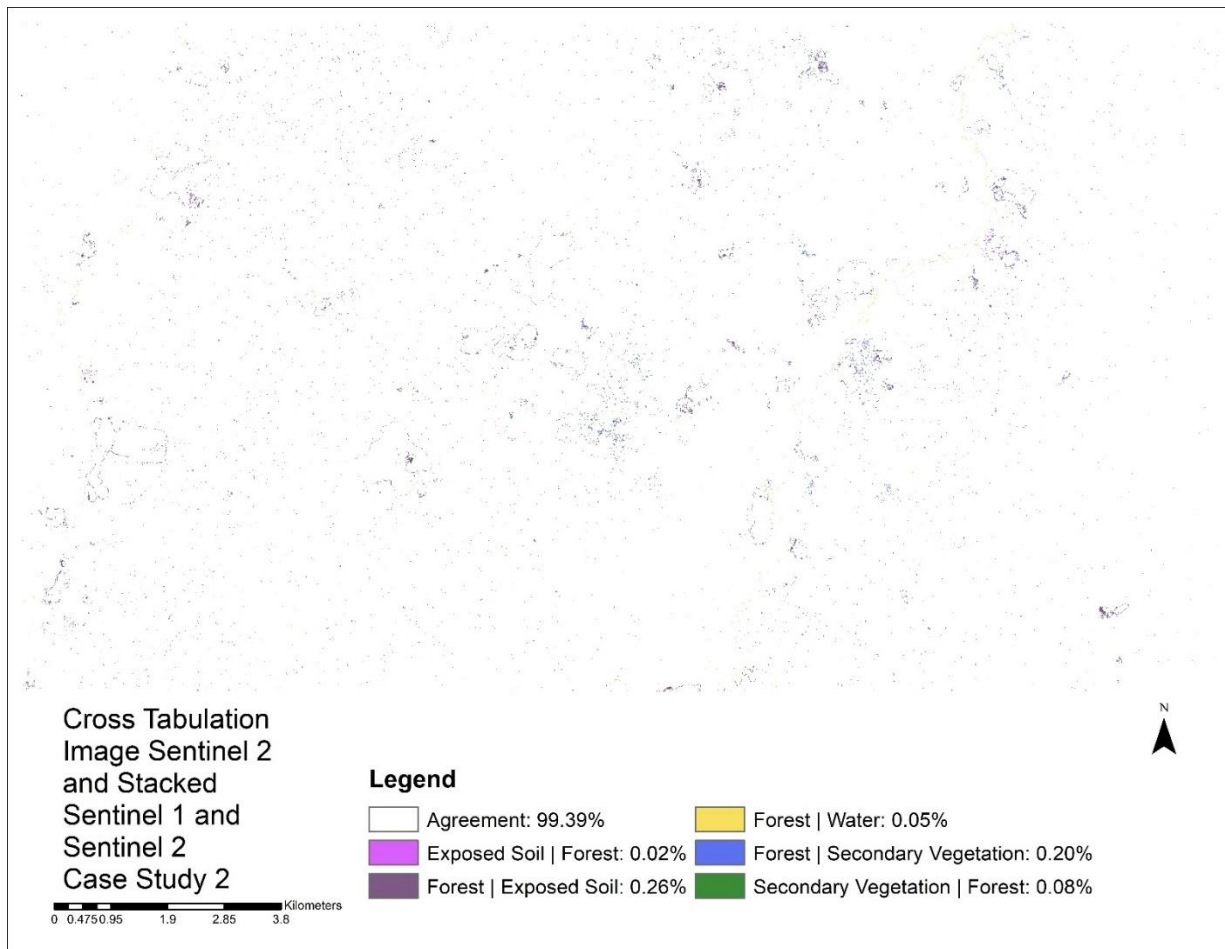


Figure 19: Cross tabulation image between Sentinel-2 and combined Sentinel-1 and -2 Case Study 2

7.1 Appendix:

Table 3: Case 1 Summary Table of Accuracy Assessment Results from 250 points. Errors of Omission and Commission are reported as well as image overall accuracy.

Class	Sentinel-1		Sentinel-2		Sentinel-1 and-2	
	Commission Error	Omission Error	Commission Error	Omission Error	Commission Error	Omission Error
Forest	10%	52%	8%	15%	11%	11%
Secondary Vegetation	60%	29%	58%	40%	46%	43%
Residential	70%	25%	26%	7%	23%	7%
Water	48%	16%	4%	14%	0%	18%
Exposed Soil	32%	29%	32%	48%	31%	31%
Overall Accuracy:	56%		74%		78%	

Table 4: Case 2 Summary Table of Accuracy Assessment Results from 200 Points. Errors of Omission and Commission are reported as well as image overall accuracy.

Class	Sentinel-1		Sentinel-2		Sentinel-1 and 2	
	Commission Error	Omission Error	Commission Error	Omission Error	Commission Error	Omission Error
Forest	6%	70%	34%	51%	24%	44%
Secondary Vegetation	98%	83%	56%	29%	46%	31%
Water	94%	0%	28%	28%	24%	14%
Exposed Soil	50%	26%	10%	12%	14%	14%
Overall Accuracy:	38%		68%		73%	

Table 5: Confusion Matrix for Case Study 1

Sentinel-1	Forest	Soil	Residential	Water	Secondary Vegetation	Total	User Accuracy
Forest	45	1	1	0	3	50	0.90
Soil	6	34	4	4	2	50	0.68
Residential	21	10	15	1	3	50	0.30
Water	0	24	0	26	0	50	0.52
Secondary Vegetation	22	8	0	0	20	50	0.40
Total	94	77	20	31	28	250	0
Producer Accuracy	0.48	0.44	0.75	0.84	0.71	0	0.56

Sentinel-2	Forest	Soil	Residential	Water	Secondary Vegetation	Total	User Accuracy
Forest	46	0	0	1	3	50	0.92
Soil	1	34	3	3	9	50	0.68
Residential	0	9	37	2	2	50	0.74
Water	2	0	0	48	0	50	0.96
Secondary Vegetation	5	22	0	2	21	50	0.42
Total	54	65	40	56	35	250	0
Producer Accuracy	0.85	0.52	0.93	0.86	0.60	0	0.74

Combined Sentinel-1 and -2	Forest	Soil	Residential	Water	Secondary Vegetation	Total	User Accuracy
Forest	48	0	0	3	3	54	0.89
Soil	1	45	3	6	10	65	0.69
Residential	0	9	37	0	2	48	0.77
Water	0	0	0	46	0	46	1
Secondary Vegetation	5	11	0	1	20	37	0.54
Total	54	65	40	56	35	250	0
Producer Accuracy	0.89	0.69	0.93	0.82	0.57	0	0.78

Table 6: Confusion Matrix Case Study 2

Sentinel-1	Exposed Soil	Forest	Water	Secondary Vegetation	Total	User Accuracy
Exposed Soil	25	24	0	1	50	0.50
Forest	0	47	0	3	50	0.94
Water	5	41	3	1	50	0.06
Secondary Vegetation	4	45	0	1	50	0.02
Total	34	157	3	6	200	0
Producer Accuracy	0.74	0.30	1	0.17	0	0.38

Sentinel-2	Exposed Soil	Forest	Water	Secondary Vegetation	Total	User Accuracy
Exposed Soil	45	3	0	2	50	0.90
Forest	0	33	14	3	50	0.66
Water	6	4	36	4	50	0.72
Secondary Vegetation	0	28	0	22	50	0.44
Total	51	68	50	31	200	0
Producer Accuracy	0.88	0.49	0.72	0.71	0	0.68

Combined Sentinel-1 and -2	Exposed Soil	Forest	Water	Secondary Vegetation	Total	User Accuracy
Exposed Soil	43	5	1	1	50	0.86
Forest	0	38	5	7	50	0.76
Water	7	2	37	4	50	0.74
Secondary Vegetation	0	23	0	27	50	0.54
Total	50	68	43	39	200	0
Producer Accuracy	0.86	0.56	0.86	0.69	0	0.73

Table 7: Cross Tabulation of Images, Case Study 1

Cross Tabulation of Sentinel-1 (Columns) and Sentinel-2 (Rows)						
Category	Forest	Exposed Soil	Residential	Water	Secondary Vegetation	Total
Forest	264995	5773	1572	71	1804	274215
Soil	17949	19524	970	435	796	39674
Residential	5105	2718	743	70	165	8801
Water	254	1637	17	376	25	2309
Secondary Vegetation	15144	3488	296	43	550	19521
Total	303447	33140	3598	995	3340	344520

Cross Tabulation of Sentinel-1 (Columns) and Combined Sentinel-1 and-2 (Rows)						
Category	Forest	Exposed Soil	Residential	Water	Secondary Vegetation	Total
Forest	264130	5392	1548	59	1778	272907
Exposed Soil	13316	22840	919	483	791	38349
Residential	5771	2131	851	30	153	8936
Water	80	1627	9	415	22	2153
Secondary Vegetation	20150	1150	271	8	596	22175
Total	303447	33140	3598	995	3340	344520

Cross Tabulation of Sentinel-2 (Columns) and Combined Sentinel-1 and -2 (Rows)						
Category	Forest	Exposed Soil	Residential	Water	Secondary Vegetation	Total
Forest	271592	392	0	118	805	272907
Exposed Soil	268	32460	906	129	4586	38349
Residential	0	1031	7857	48	0	8936
Water	19	94	37	2000	3	2153
Secondary Vegetation	2336	5697	1	14	14127	22175
Total	274215	39674	8801	2309	19521	344520

Table 8: Cross Tabulation of Images, Case Study 2

Cross Tabulation Between Sentinel-1 (Columns) and Sentinel-2 (Rows)					
Category	Exposed Soil	Forest	Water	Secondary Vegetation	Total
Exposed Soil	22893	44640	11	41	67585
Forest	27215	2188725	83	337	2216360
Water	102	441	1	0	544
Secondary Vegetation	63	5051	0	9	5123
Total	50273	2238857	95	387	2289612

Cross Tabulation of Sentinel-1 (Columns) and Combined Sentinel-1 and-2 (Rows)					
Category	Exposed Soil	Forest	Water	Secondary Vegetation	Total
Exposed Soil	23699	49259	12	44	73014
Forest	26077	2180684	78	335	2207174
Water	299	1269	4	0	1572
Secondary Vegetation	198	7645	1	8	7852
Total	50273	2238857	95	387	2289612

Cross Tabulation of Sentinel-2 (Columns) and Combined Sentinel-1 and-2 (Rows)					
Category	Exposed Soil	Forest	Water	Secondary Vegetation	Total
Exposed Soil	66996	5994	24	0	73014
Forest	570	2204782	6	1816	2207174
Water	19	1039	514	0	1572
Secondary Vegetation	0	4545	0	3307	7852
Total	67585	2216360	544	5123	2289612

Literature Cited:

1. Abdikan S., Sanli F.B., Ustnuner M., Calo F., "Land Cover Mapping Using Sentinel-1 SAR Data". Photogrammetry, Remote Sensing and Spatial Information Services, Volume XLI-B7, 2016 XXIII ISPRS Congress, 12-19 July 2016, Pargue, Czech Republic.
2. Breiman, L. Machine Learning (2001) 45: 5. <https://doi.org/10.1023/A:1010933404324>

3. UNFCCC. 2014. Key decisions relevant for reducing emissions from Deforestation and forest degradation in developing countries (REDD+). Decision Booklet REDD+. UNFCCC Publication: Bonn, Germany.
4. Bourg, L. (2009): MERIS Level 2 Detailed Processing Model. ACRI-ST, Document No. PO-TN-MEL-GS-0006, 15 July 2009.
5. Nicola Clerici, Cesar Augusto Valbuena Calderón & Juan Manuel Posada (2017) Fusion of Sentinel-1A and Sentinel-2A data for land cover mapping: a case study in the lower Magdalena region, Colombia, *Journal of Maps*, 13:2, 718-726, DOI:10.1080/17445647.2017.137231
6. Chuvieco Emilio. 2016. *Fundamentals of Satellite Remote Sensing: An Environmental Approach*. Second Edition. Taylor & Francis Group. Boca Raton, Florida. 2016.
7. Dostálová Alena, Hollaus Markus, Milenković Milutin, and Wagner Wolfgang (2016). Forest area derivation from Sentinel-1 data. *Remote Sensing and Spatial Information Sciences*, 3:7, 12-19, DOI: [10.5194/isprs-annals-III-7-227-2016](https://doi.org/10.5194/isprs-annals-III-7-227-2016)
8. "ESA, Copernicus, Overview". ESA. 28 October 2014. Retrieved 26 April 2016.
9. Yolanda Fernandez-Ordonez, Jesus Soria-Ruiz and Brigitte Leblon (2009). Forest Inventory using Optical and Radar Remote Sensing, *Advances in Geoscience and Remote Sensing*, Gary Jedlovec (Ed.), ISBN: 978-953-307-005-6, InTech, Available from: <http://www.intechopen.com/books/advances-in-geoscience-and-remote-sensing/forestinventory-using-optical-and-radar-remote-sensing>
10. Gerald Forkuor, Kangbeni Dimobe, Idriss Serme & Jerome Ebagnerin Tondoh (2018) Landsat-8 vs. Sentinel-2: examining the added value of sentinel-2's red-edge bands to land-use and land-cover mapping in Burkina Faso, *GIScience & Remote Sensing*, 55:3, 331-354, DOI: 10.1080/15481603.2017.1370169
11. Funning, G. (2018). *Insar Theory and Processing* [Powerpoint slides]. Retrieved from: <https://www.unavco.org/education/professional-development/short-courses/2018/insar-training-gsa/insar-training-gsa.html>
12. Google earth V 6.2.2.6613. (July , 2018). Pando Department, Bolivia. 10° 25' 35.27"S, 67° 27' 51"W, Eye alt 29 mi. DigitalGlobe 2018. <http://www.earth.google.com> [September, 2018].
13. *Global forest resources assessment 2015: Desk reference*. FAO. Book. URI: <http://www.fao.org/3/a-i4808e.pdf> · <http://hdl.handle.net/20.500.11822/19698>.

14. M. Hansen, R. Dubaya & R. Defries (1996) Classification trees: an alternative to traditional land cover classifiers, *International Journal of Remote Sensing*, 17:5, 1075-1081, DOI: 10.1080/01431169608949069
15. Barry Haack and Ron Mahabir (2018) Relative value of radar and optical data for land cover/use mapping: Peru example, *International Journal of Image and Data Fusion*, 9:1, 1-20, DOI: [10.1080/19479832.2017.1398188](https://doi.org/10.1080/19479832.2017.1398188)
16. Terry Idol, Barry Haack, and Ron Mahabir (2015) Comparison and integration of spaceborne optical and radar data for mapping in Sudan, *International Journal of Remote Sensing*, 36:6, 1551-1569, DOI: [10.1080/014131161.2015.1015659](https://doi.org/10.1080/014131161.2015.1015659)
17. Kasischke, E. S., Melack, J. M., & Dobson, M. C. (1997). The use of imaging radars for ecological applications—A review. *Remote Sensing of Environment*, 59, 141–156.
18. Laur H., Bally P., Meadows P., Sinchez J., Schittler B., Lopinto E. & Esteban D., ERS SAR Calibration: Derivation of σ_0 in ESA ERS SAR PRI Products, ESA/ESRIN, ES-TN-RS-PM-HL09, Issue 2, Rev. 5f, November 2004
19. Lee, J.-S., Jurkevich, I., Dewaele, P., Wambacq, P., and A. Oosterlinck, 1994, "Speckle Filtering of Synthetic Aperture Radar Images: A Review," *Remote Sensing Review*, 8:313-340.
20. Lee, J.S., 1981. Speckle Analysis and Smoothing of Synthetic Aperture Radar Images. *Computer Graphics and Image Processing*, Vol. 17:24-32.
21. Li L., Roy D., (2017). A Global Analysis of Sentinel-2A, Sentinel-2B, and Landsat-8 Data Revisit Intervals and Implications for Terrestrial Monitoring. *Remote Sensing*, 9, 902; doi: 10.3390/rs9090902. www.mdpi.com/journal/remotesensing.
22. Mansourpour M., Rajabi M.A., Blais J.A.R., 2006, "Effects and Performance of Speckle Noise Reduction Filters on Active Radar and SAR Images", <http://people.ucalgary.ca/~blais/Mansourpour2006.pdf>
23. Morley, R. J. 2000. *Origin and Evolution of Tropical Rain Forests*, Chichester: John Wiley and Sons. p. 362, 378.
24. Müller R, Pacheco P and Montero JC. 2014. The context of deforestation and forest degradation in Bolivia: Drivers, agents and institutions. Occasional Paper 108. Bogor, Indonesia: CIFOR.
25. Mitchell A, Rosenqvist A, Mora B. 2017. Current remote sensing approaches to monitoring forest degradation in support of countries measurement, reporting and verification (MRV) systems for REDD+. *Carbon Balance and Management*. Published Online. 17 April 2017.

26. Magangoz A., Sekertekin A., Akcin H. "Analysis of Land Use Land Cover Classification Results Derived From Sentinel-2 Image". Photogrammetry and Remote Sensing. 2017.
27. M. Mahmudur Rahmanm, Tetuko Sri Sumantyo J., "Mapping Tropical Forest Cover and Deforestation Using Synthetic Aperature Radar (SAR) Images". Appl Geomat (2010) 2:113-121. DOI: 10.1007/s12518-010-0026-9.
28. E. Mandanici and G. Bitelli., (2016) "Preliminary Comparison of Sentinel-2 and Landsat 8 Imagery for a Combined Use". Remote Sensing, 8, 1014. Doi:10.3390/rs8121014.
29. Kuhn, M. (2008). Building Predictive Models in R Using the caret Package. Journal of Statistical Software, 28(5), 1 - 26. doi:http://dx.doi.org/10.18637/jss.v028.i05
30. Pistorius T. From RED to REDD+: the evolution of a forest-based mitigation approach for developing countries. Curr Opin Environ Sustain. 2012;4(6):638-45.
31. Qiu F., Berglund J., Jensen J., Thakkar P., and Ren D., 2004, "Speckle Noise Reduction in SAR Imagery Using a Local Adaptive Median Filter". *GIScience and Remote Sensing*, Vol. 41:244-266.
32. Johannes Reiche, Eliakim Hamunyela, Jan Verbesselt, Dirk Hoekman, Martin Herold (2018) Improving near-real time deforestation monitoring in tropical dry forests by combining dense Sentinel-1 time series with Landsat and ALOS-2 PALSAR-2. Remote Sensing of Environment, 204: 147-161.
33. SNAP - ESA Sentinel Application Platform v6.0.5, <http://step.esa.int>
34. Sawaya, S., B. Haack, T. Idol, and A. Sheoron. 2010. "Land Use/Cover Mapping with Quad-Polarization RADAR and Derived Texture Measures Near Wad Madani, Sudan." *GIScience & Remote Sensing* 47 (3): 398-411. Doi: 10.2747/1548-1603.47.3.398
35. Shearon, A., and B. Haack. 2013. "Classification of California Agriculture using Quad Polarization Radar Data and Landsat Thematic Mapper Data." *GIScience and Remote Sensing* 50 (1): 50-63. Doi: 10.1080/15481603.2013.778555.
36. Smith, R. B. 2012. *Interpreting Digital Radar Images with Tntmips*, 20. Lincoln, NE: MicroImages.
37. Sentinel-1 Observation Scenario. Web Access 4/12/2018. url: <https://sentinel.esa.int/web/sentinel/missions/sentinel-1/observation-scenario>
38. Sentinel-2 Revisit and Coverage. Web Access 4/12/2018. url: <https://earth.esa.int/web/sentinel/user-guides/sentinel-2-msi/revisit-coverage>
39. Skinner B. and Murck B. (2011). "The Blue Planet: an introduction to earth system science". John Wiley & Sons, Inc.
40. Small D., Schubert A., Guide to ASAR Geocoding, RSL-ASAR-GC-AD, Issue 1.0, March 2008

41. Suhet, B. Hoersch, "Sentinel-2 User Handbook" (2015). European Space Agency (ESA).
https://sentinel.esa.int/documents/247904/685211/Sentinel-2_User_Handbook
42. Schmullius, C.; Thiel, C.; Pathe, C.; Santoro, M. Radar time series for land cover and forest mapping. In *Remote Sensing Time Series*; Kuenzer, C., Dech, S., Wagner, W., Eds.; Remote Sensing and Digital Image Processing; Springer International Publishing: Basel, Switzerland, 2015; pp. 323–356
43. Violini Soraya., (2013). *Deforestation: Change Detection in Forest Cover Using Remote Sensing*. Maio-Gulich Insitute, CONAE. Argentina.
44. Thanh Noi, P.; Kappas, M. Comparison of Random Forest, k-Nearest Neighbor, and Support Vector Machine Classifiers for Land Cover Classification Using Sentinel-2 Imagery. *Sensors* 2018, 18, 18.
45. Thiel, C.; Cartus, O.; Eckardt, R.; Richter, N.; Thiel, C.; Schmullius, C. Analysis of multi-temporal land observation at C-band. In *Proceedings of the 2009 IEEE International Geoscience and Remote Sensing Symposium (IGARSS)*, Cape Town, South Africa, 12–17 July 2009; doi:10.1109/IGARSS.2009.5417764.
46. Waske B., Braun M., Classifier ensembles for land cover mapping using multitemporal SAR imagery (2009), *Journal of Photogrammetry and Remote Sensing*, 64:5, 450-457,
<https://doi.org/10.1016/j.isprsjprs.2009.01.003>
47. T. Warner, M. Nellis, G. Foody, (2009) "*The SAGE Handbook of Remote Sensing*". SAGE Publications Ltd.
48. Wang, B.; Jia, K.; Liang, S.; Xie, X.; Wei, X.; Zhao, X.; Yao, Y.; Zhang, X. Assessment of Sentinel-2 MSI Spectral Band Reflectances for Estimating Fractional Vegetation Cover. *Remote Sens.* **2018**, 10, 1927.